



Distinguishing between basalts produced by endogenic volcanism and impact processes: A non-destructive method using quantitative petrography of lunar basaltic samples

Clive R. Neal^{a,b,c,*}, Patrick Donohue^{a,b}, Amy L. Fagan^{a,b,c}, Katie O'Sullivan^{a,b}, Jocelyn Oshrin^a, Sarah Roberts^{a,b}

^a Department of Civil & Env. Eng. & Earth Sciences, University of Notre Dame, Notre Dame, IN 46556, USA¹

^b NASA Lunar Science Institute, USA

^c Center for Lunar Science and Exploration, Lunar and Planetary Institute, 3600 Bay Area Boulevard, Houston, TX 77058, USA

Received 28 February 2014; accepted in revised form 17 August 2014; available online 27 August 2014

Abstract

Impact processes play an important role in shaping and reshaping the surfaces of airless planetary bodies. Such processes produce regoliths and generate melts that crystallize and record the homogenization of the geology at the impact site. If the volume of melt is substantial, the resultant crystallized product has an igneous texture and may be free of xenolithic clasts making it difficult to distinguish from melts produced by endogenic magmatic processes. This has been clearly demonstrated during the return of the Apollo samples from the Moon, where Apollo 14 basalt 14310 was initially described as a mare basalt and was only subsequently reclassified as an impact melt following detailed and time consuming crystallization experiments. Another way of distinguishing lunar impact melts from endogenically-derived mare basalts is through the quantification of the highly siderophile elements (HSE: Pd, Rh, Ru, Ir, Pt, Os), which have relatively low abundances in pristine lunar samples but are high in meteorites and, therefore, may be enriched in impact melts. However, these analyses consume relatively large quantities of valuable sample and because of mass constraints cannot be performed on many lunar samples. In this paper we present a quantitative petrographic method that has the potential to distinguish lunar impact melts from endogenically-derived mare basalts using plagioclase and olivine crystal size distributions (CSDs). The slopes and intercepts of these CSDs are used to show that olivine from impact melts displays a steeper CSD relative to olivine from mare basalts. For plagioclase, generally impact melts display CSDs with shallower gradients than those from endogenous mare basalts and, as for olivines, plot in a distinct field on a CSD slope vs. CSD intercept plot. Using just a thin section to distinguish impact melts from mare basalts enables the goals of future robotic sample return missions to determine the age of the South Pole-Aitken basin in the Moon, because such missions will potentially only return small (2–4 mm) “rocklets” for analysis, obviating HSE analyses for impact melt identification.

© 2014 Elsevier Ltd. All rights reserved.

1. INTRODUCTION

Basaltic samples returned from the Moon can have distinctly different origins through endogenic volcanism (producing pristine mare basalts) or through impact melting processes, and distinguishing between these origins on the basis of texture is difficult. As an illustrative example,

* Corresponding author at: Department of Civil & Env. Eng. & Earth Sciences, University of Notre Dame, Notre Dame, IN 46556, USA.

E-mail address: neal.1@nd.edu (C.R. Neal).

¹ Formerly the Department of Civil Eng. & Geological Sciences.

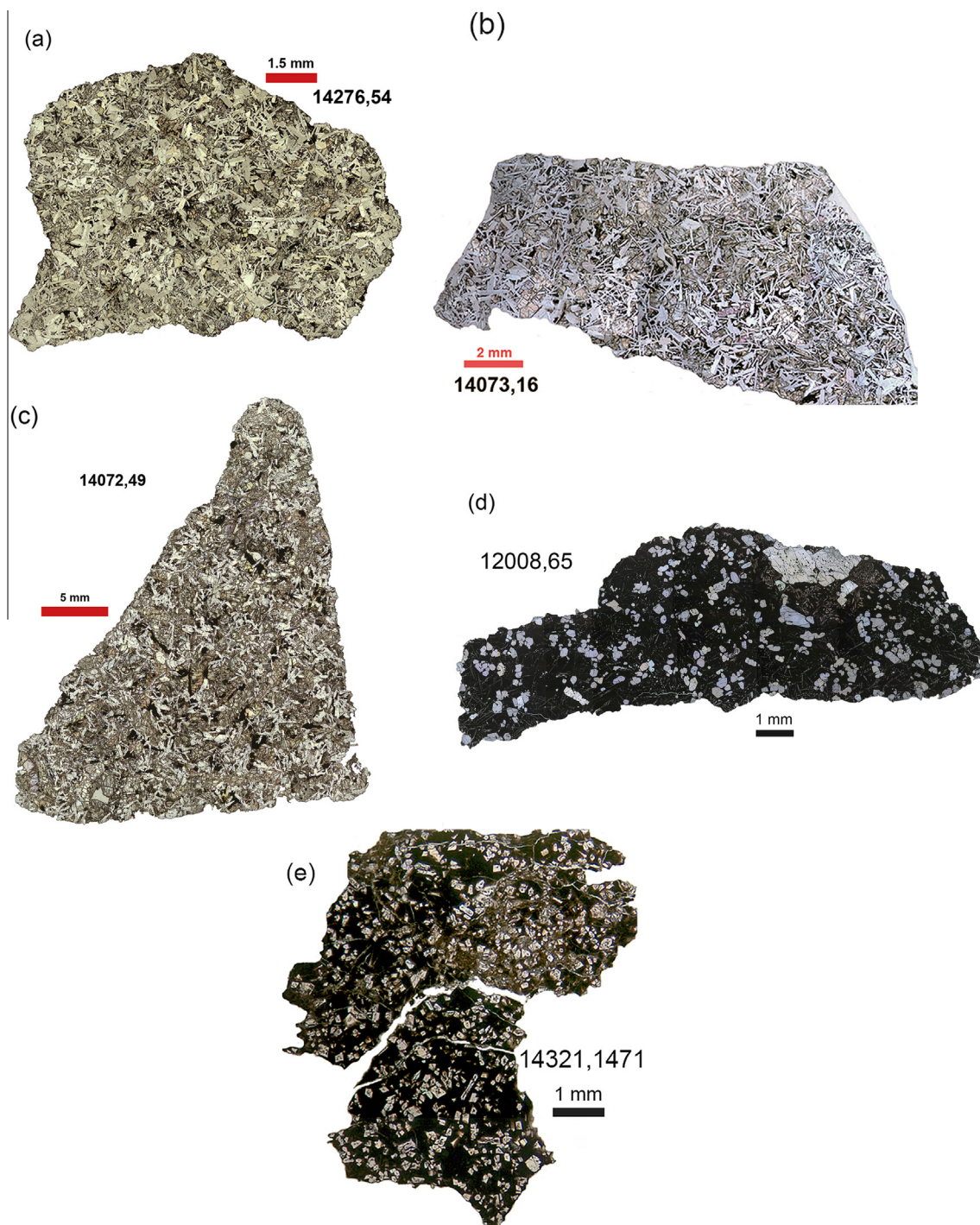


Fig. 1. Photomicrographs of (a) impact melt 14276, (b) impact melt 14073, (c) pristine mare basalt 14072, (d) pristine mare basalt 12008,65, and (e) Apollo 14 olivine vitrophyre (impact melt) 14321,1471. All photomicrographs are in plane polarized light. Qualitative comparison of the plagioclase textures in (a), (b), and (c), as well as olivine in (d) and (e), cannot distinguish one from the other.

the textures of two Apollo 14 impact melts (14073 and 14276; Fig. 1a and b, respectively) appear texturally similar to a pristine mare basalt (14072) (Fig. 1c). Furthermore, although basaltic sample 14310 was originally classified as a pristine high-Al mare basalt (e.g., Longhi et al., 1972; Ridley et al., 1972; Crawford and Hollister, 1974),

subsequent experimental studies of dynamic crystallization demonstrated its impact origin (e.g., Usselman and Lofgren, 1976; Lofgren, 1977). Traditionally, such distinctions required time consuming experiments (e.g., Usselman and Lofgren, 1976; Lofgren, 1977), or destructive analyses using relatively large quantities (0.4 g to >1.0 g) of

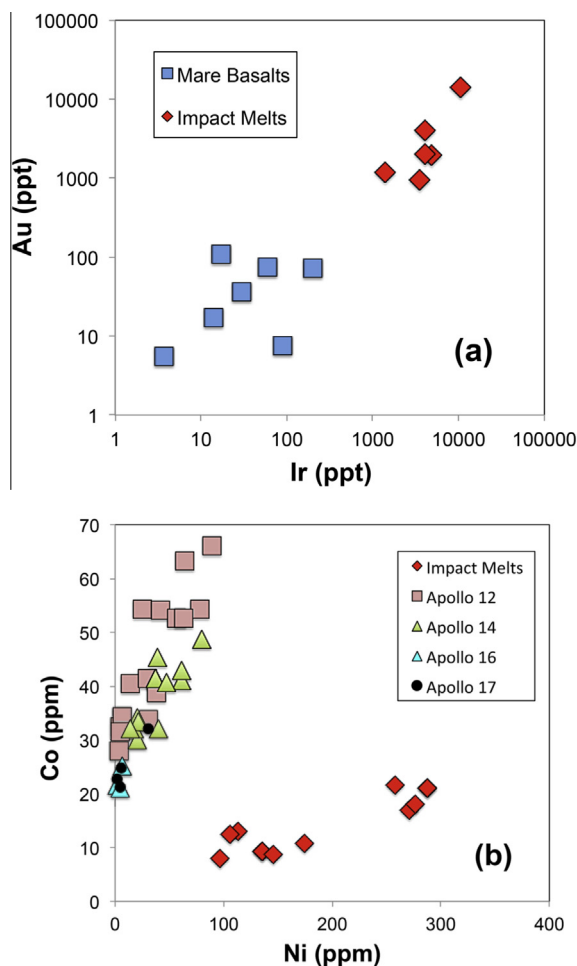


Fig. 2. Siderophile element abundances in the samples being studied in this paper. (a) Ir vs. Au abundances demonstrating that the impact melts used in this study have much higher abundances; (b) Ni vs. Co plot showing that impact melts have higher Ni and lower Co abundances than endogenous mare basalts. Data from: Baedeker et al. (1972), Ebihara et al. (1992), Ehmann et al. (1972), Fagan et al. (2013b), Fischer-Godde and Becker (2012), Hertogen et al. (1977), Hubbard et al. (1972), Krahenbuhl et al. (1973), Laul et al. (1972), Longhi et al. (1972), Morgan et al. (1972), Neal (2001), Neal and Kramer (2006), Neal et al. (1988ab), Philpotts et al. (1972), Palme et al. (1978), Rose et al. (1972), Ryder and Norman (1980), Shervais et al. (1985b), Taylor et al. (1972), Vaniman and Papike (1980), Warren and Wasson (1978), Willis et al. (1972).

material to determine the highly siderophile element (HSE) abundances of the samples (e.g., Anders et al., 1971; Anders, 1978; Wolf et al., 1979). It has been demonstrated that pristine lunar samples contain HSE abundances that are exceedingly low in the pg/g range (e.g., Righter et al., 2000; Walker et al., 2004; Day et al., 2007, 2010). As meteorites contain much higher HSE abundances (mg/g in some cases), impact melts usually have HSE abundances in the ng/g to mg/g range (e.g., Morgan et al., 1974; Puchtel et al., 2008), although inefficient mixing during the impact process could melt impact melts do not exhibit such enrichments. Warren and Wasson (1977) proposed parameters for

identifying pristine non-mare rocks, which included: low siderophile and non-KREEP-like incompatible element concentrations (“siderophile contents $\sim 3 \times 10^{-4}$ times or less than those in CI chondrites provide the most reliable evidence for pristinity”); coarse granularity, phase homogeneity, coarse exsolution lamellae, cumulate textures; and radiometric ages ~ 4.2 Ga. Warren (1993) produced a compilation of 260 non-mare samples that used petrologic and geochemical characteristics (mainly texture and siderophile element abundances) and produced seven categories of confidence for the pristinity of a given sample. However, textural analyses were only qualitative and emphasis was instead placed on the destructive analyses of the samples to determine HSE abundances (Warren and Wasson, 1977; Warren, 1993). However, Wolf et al. (1979) analyzed mare basalts and highlands rocks for HSE and volatile elements and noted that mare basalts had higher abundances than predicted by Delano and Ringwood (1978), who attempted to predict the abundances of siderophiles in a primary plagioclase crust that crystallized from the lunar magma ocean.

While HSE abundances are a potentially good indicator of a non-pristine origin of impact melt rocks (although not an absolute indicator; e.g., Warren, 1993), not all returned samples are large enough to allow accurate HSE abundances to be determined (e.g., breccia clasts, rake samples, etc.). Given that in the near future any sample return mission to the Moon (or any other planetary body) will be robotic in nature, the sample masses will be small. Furthermore, the National Research Council (2007) placed understanding the bombardment history of the inner Solar System as uniquely revealed by the Moon as its top priority for lunar science. This is reflected in the current NASA Planetary Sciences Division Decadal Survey (National Research Council, 2011) where a sample return from South Pole Aitken basin to determine the age of the impact is a named, high priority New Frontiers class mission. Identification of impact melt samples in the sample return cache is paramount for achieving the goals of the mission. As this robotic sample return mission will collect rake samples, it is unlikely that sufficient sample will be available for HSE determinations and accurate age determinations. Therefore, building on the experimental studies from the 1970s noted above for 14310 (Usselman and Lofgren, 1976; Lofgren, 1977), textures will need to be used to distinguish basaltic samples derived from impacts vs. endogenic volcanism. A textural method that will achieve this is presented here.

Quantitative textural studies of impact-generated rocks have been conducted previously, but have focused on clast-size distributions, rather than crystal-size distributions. For example, Pittarello and Koeberl (2013) used a similar quantitative petrographic approach to study impact lithologies from the El’gygytyn impact structure in Arctic Russia. As the site contained a variety of volcanic lithologies, the clast size distribution method they developed could not be applied to distinguish impact and unshocked lithologies. Pittarello and Koeberl (2013) focused on the suevite to define lithic clast size distributions by their geometric properties and found the method allowed the classification of unshocked to slightly shocked volcanic clasts included in

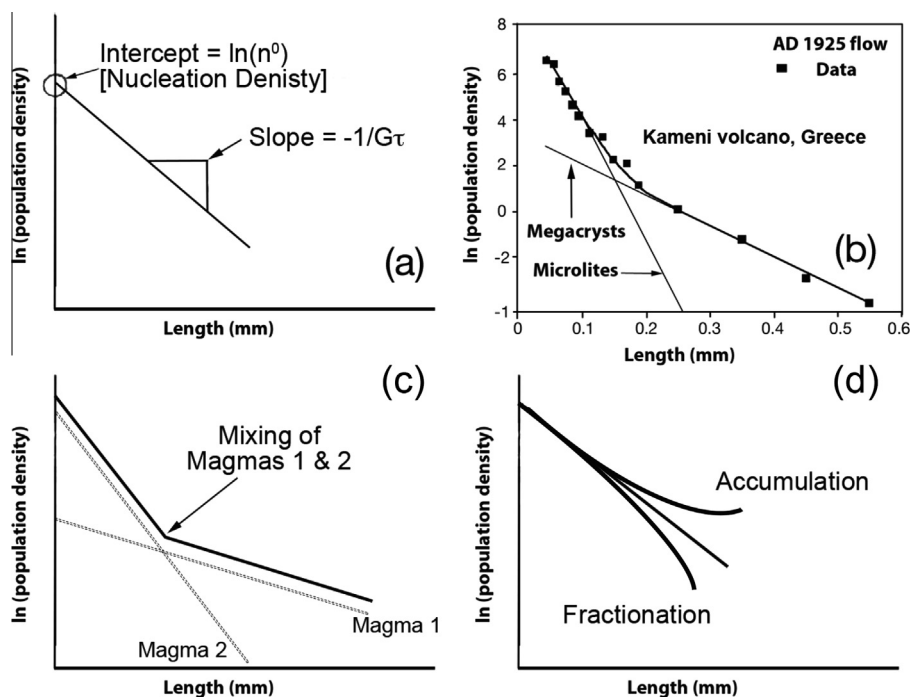


Fig. 3. Anatomy of a crystal size distribution. (a) Slope and intercept definitions (modified from Marsh, 1998) showing the CSD gradient is proportional to the crystal growth rate and residence time, with the y-intercept equivalent to the nucleation density; (b) explanation of a “kinked” CSD (modified from Higgins, 1996) where two crystal populations grow in response to different cooling rates within the same magma; (c) kinked CSDs can also indicate magma mixing where the two magmas crystallized the same phase but at different cooling rates prior to mixing; (d) curved CSDs can reflect crystal fraction or accumulation as shown.

the suevite. Other examples include the clast size distributions in pseudotachylytes (Shimamoto and Nagahama, 1992; Tsutsumi, 1999) and impactites (e.g., Chanou et al., 2014).

This paper presents a quantitative petrographic method that distinguishes basaltic samples formed through endogenic processes from those formed by impacts using olivine and plagioclase crystal size distributions (CSDs). Comparison of the slopes and y-axis intercepts of these CSDs allows the distinction to be made between the two petrogeneses and builds upon the work of several recent contributions (Oshrin, 2009; Oshrin and Neal, 2009; Hui et al., 2011; Fagan, 2012; O’Sullivan, 2012; Fagan et al., 2013a; and Fagan and Neal, 2012; Donohue, 2013). During these studies, it has been demonstrated that phenocrysts can be distinguished from xenocrysts in impact melts by texture and composition (e.g., Figs. 3–5 in Fagan et al., 2013a,b). This work represents a culmination of 6 years work by current and former Notre Dame graduate students (and coauthors on this paper) in constructing CSDs as part of their respective degree projects.

2. SAMPLES

Plagioclase is ubiquitous in both pristine mare basalts and impact melts; olivine is an early crystallizing phase in some mare basalts and impact melts. Building upon the work reported by Oshrin (2009), Hui et al. (2011), Neal et al. (2010), Fagan and Neal (2012), and Donohue

(2013), plagioclase CSDs have been constructed for mare basalts (see Table 1 for specific thin sections) from Apollo 12 ($N=14$), 14 ($N=20$), 16 ($N=5$), and 17 ($N=9$), as well as for basaltic impact melts from Apollo 14 ($N=3$) and 16 ($N=9$). None of these samples exhibit an alignment of crystals indicating they represent a random sampling of crystals that exhibit no flow texture. Complementing the work of Fagan et al. (2013a), olivine CSDs (Table 2) have also been constructed for additional Apollo 12 ($N=5$), Apollo 14 ($N=3$), Apollo 16 ($N=2$) and Apollo 17 ($N=7$) basalts as well as for known Apollo 14 impact melts (olivine vitrophyres $N=4$; described as impact melts by Allen et al., 1979; Shervais et al., 1988). The mare basalts used in this study represent samples from the Apollo 12 pigeonite and ilmenite basalt suites plus the one feldspathic basalt (12038) (Neal et al., 1994a,b); each geochemical group of the Apollo 14 high-Al basalts (Neal and Kramer, 2006) excluding the very high potassium basalts (“VHK”- Shervais et al., 1985a; Neal et al., 1988a, 1989a,b); three Apollo 16 basalts (Zeigler et al., 2006; Fagan and Neal, 2012); and each geochemical group from the Apollo 17 mare basalts (Rhodes et al., 1977; Neal et al., 1990; Ryder, 1990). Detailed petrographic descriptions for each sample have been previously reported in the literature and the relevant references are contained within Tables 1 and 2.

Not all of the samples analyzed have been analyzed for the highly siderophile elements. All siderophile element data that have been published for the samples studied here

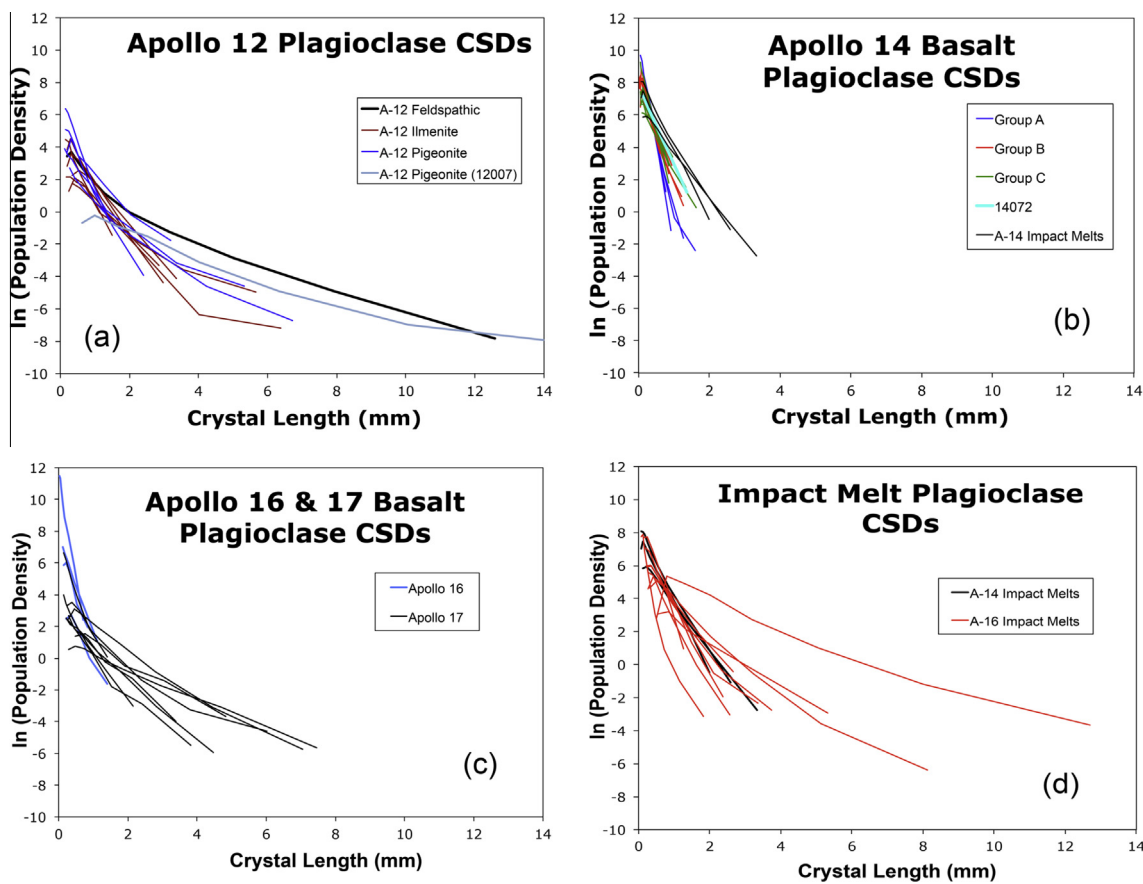


Fig. 4. Plagioclase CSDs for mare basalts and lunar impact melts. (a) Basalts returned by the Apollo 12 mission; (b) basalts returned by the Apollo 14 mission; (c) basalts returned by the Apollo 16 and 17 missions; (d) impact melts returned by the Apollo 14 and 16 missions.

are represented in Fig. 2. For the highly siderophile elements Au and Ir (Fig. 2a), the impact melts contain 1–2 orders of magnitude more than the mare basalts. Substantially more data are available when Ni and Co are considered (Fig. 2b). The impact melts contain substantially different Ni/Co ratios than the mare basalts (8–17 vs. <2) as they contain generally higher Ni and lower Co abundances than mare basalts. Fig. 2 demonstrates that the samples we are classifying as impact melts and endogenous mare basalts have chemical compositions consistent with that classification.

3. METHOD

Crystal size distributions (CSDs) are used to quantify population densities within particular size bins of a given mineral phase and have been developed to define crystallization history for terrestrial samples (e.g., Cashman and Marsh, 1988; Marsh, 1988, 1998; Cashman, 1990). To construct a CSD in this study, individual crystals of a given phase were traced from thin section digital photomicrograph mosaics using *Adobe Photoshop*[®] and the outline of the entire section was also traced. Minerals that intersected the edge of the thin section were omitted, as they do not represent complete crystals. The resulting crystal layers were imported into *ImageJ* (Rasband, 1997; Higgins and

Chandrasekharam, 2007), which measures the major and minor axes, roundness, and area of each crystal. *ImageJ* is used in preference over the older *ImageTool* (Higgins, 2000) because *ImageJ* can accommodate larger image file sizes, thus better retaining the integrity of the smallest crystals. Individual crystals with minor axes <0.03 mm are likely to be a projection of a crystal rather than an accurate measurement due to the approximately equivalent thickness of the thin-section (Higgins, 2000) and a downturn (positive slope) in the CSD is usually seen at these small sizes. Processing of the two-dimensional thin section image to a three-dimensional representation requires the extraction of parameters that describe the intersections of the individual crystals (e.g., length, width, area, perimeter, orientation and centroid location) with the plane of thin section. The major and minor axes of crystals were imported into *CSDslice* (Morgan and Jerram, 2006) to determine the best-fit short, intermediate, and long axes of the 3-D crystal habit. These data, in conjunction with the major and minor axes, individual crystal area, average crystal roundness, and total sample area, were used in *CSDcorrections* 1.39 (Higgins, 2000, 2002a; Higgins and Chandrasekharam, 2007) to determine the 3-D CSD using 5 bins per decade (i.e., per log unit). Higgins (2000) reported that using more than 5 bins per decade can introduce errors because (1) there are fewer crystals in each bin,

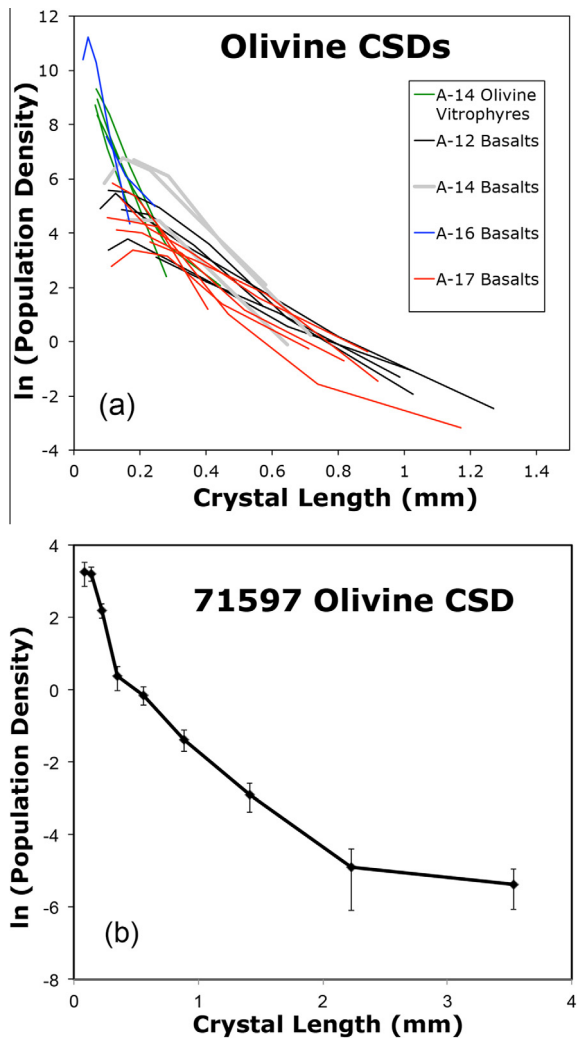


Fig. 5. (a) Olivine CSDs from basalts returned by the Apollo 12, 14, and 17 missions as well as two basaltic samples from Apollo 16 (Zeigler et al., 2006) and Apollo 14 olivine vitrophyres (impact melts) (Fagan et al., 2013a); (b) CSD for basaltic sample 71597, an olivine cumulate (Warner et al., 1977) including Population Density errors.

and (2) more cycles of correction are needed during stereological conversion. Finally, CSDs are traditionally plotted as the natural log of the population density (number of crystals of a given size per unit volume of rock) against the corrected crystal size length (Cashman and Marsh, 1988; Marsh, 1988). Corrected crystal size length allows the correction of the intersection-probability effect during the examination of a 2D plane (thin section) and how 3D non-spherical crystals intersect it. Higgins (2000) discussed the various methods (direct and indirect) for correcting the stereological affect and noted that Peterson (1996) first applied a correction to CSD data for the intersection-probability effect.

The *CSDcorrections* program also reports errors (summarized below from Higgins, 2000) on the population density for each size bin on the basis of the:

- (1) *Counting Error*: the square root of the number of crystals within an interval (usually only significant for larger crystal sizes where the number of crystals is smaller).
- (2) *Shape Probability Parameters*: applied when converting the 2D thin section to a 3D representation. The *Probability Parameters* are precisely defined for fixed convex shapes, but most crystals are irregular or have variable shapes so it is difficult to estimate the contributions from this to the total error. However, it is relatively easy to estimate the counting errors of other intersections with the plane of the thin section and assess their impact on the total correction of a given interval. This source of error is most important for small crystal sizes.
- (3) *Conversion to Crystal Lengths*: occurs in the conversion of intermediate (for the length of crystals that intersect the plane of the thin section) or short crystal dimensions (for intersection width measurements) to crystal lengths. This will produce systematic errors in population density and the size.

The slope of a CSD is proportional to $-1/G$ (growth rate) multiplied by τ (residence time) (Fig. 3a). Crystal nucleation rate generally increases with time as an initially wholly molten package of magma cools (Cashman, 1990) and will produce a linear CSD if the cooling rate remains constant (Higgins, 2000). The intersection of the CSD with the y -axis represents the nucleation density (Fig. 3a). Non-linear CSDs indicate that dynamic and/or kinetic processes affected crystallization and produced a change in cooling rates and nucleation density (Cashman, 1990; Marsh, 1998). Crystals formed at depth (“slow” cooling) carried in the initial magma may vary in size and can easily be recognized as phenocrysts crystallized from the present host magma (Marsh, 1996, 2002), whereas the groundmass phase is much smaller and formed at a “fast” cooling rate at the surface. This produces an overall “kinked” CSD for the rock (e.g., Fig. 3b), with the larger crystals (“mega-crystals” in Fig. 3b) forming the shallower sloped portion of the CSD and the smaller crystals forming the steeper sloped limb of the CSD. Kinked CSD profiles can also be achieved through magma mixing if, prior to mixing, both magmas were crystallizing the same phase at different cooling rates (Fig. 3c). Curved CSDs (Fig. 3d) may reflect the different nucleation and growth conditions of distinct crystal populations in the rock (e.g., Higgins, 1996; Marsh, 1998; Higgins and Roberge, 2003). For example, if a magma has experienced crystal fractionation, the removal of larger crystal sizes yields a concave-down CSD profile (Fig. 3d), whereas crystal accumulation would produce a concave-up CSD profile (Fig. 3d) (Higgins, 2000).

For the method presented here, samples containing a variety of crystal sizes need to be compared with each other. Therefore, only a portion of each CSD is used and that is the portion that is present in all samples. For olivine, only the portion of the CSD that is ≤ 0.4 mm and has a negative slope is used, omitting any change in gradient that can occur in small crystal sizes. The calculated intercept of this slope is equivalent to the nucleation density (Fig. 3a;

Table 1

Samples where plagioclase crystal size distributions have been determined for this study.

Sample #	Sample Type	Al ₂ O ₃ (wt.%)	MgO (wt.%)	Petrography Reference	Whole Rock Reference	CSD Slope	CSD Intercept	Residence Time (Yrs.)	# of Crystals
12038,254	Feldspathic	12.45	6.83	[1]	[23]	-1.27	3.09	19.2	2198
<i>12016,41</i>	<i>Ilmenite</i>	<i>7.23</i>	<i>12.65</i>	<i>[2]</i>	<i>[25]</i>	<i>-2.86</i>	<i>3.30</i>	<i>8.5</i>	<i>92</i>
12051,58	Ilmenite	9.95	6.82	[2]	[24]	-2.34	3.96	10.4	1940
12054,126	Ilmenite	10.47	6.76	[2]	[25]	-1.98	2.61	12.3	563
12056,21	Ilmenite	8.82	9.3	[2]	[25]	-5.02	5.22	4.9	145
12062,13	Ilmenite	10.3	8.1	[3]	[26]	-2.95	4.77	8.3	726
12063,24	Ilmenite	9.27	9.56	[2]	[23,27]	-3.92	5.50	6.2	658
12007,17	Pigeonite	11.28	5.86	[4]	[25]	-0.83	0.56	29.2	272
12017,25	Pigeonite	10.02	7.63	[4]	[26]	-5.37	6.27	4.5	1421
12019,5	Pigeonite	9.6	9.2	[4]	[25]	-6.19	7.46	3.9	872
12021,139	Pigeonite	10.55	7.6	[4]	[28]	-2.42	3.21	10.1	614
12031,45	Pigeonite	12.63	7.13	[1]	[25]	-3.10	4.26	7.9	290
12039,4	Pigeonite	10.52	5.75	[4]	[25]	-2.44	3.08	10.0	369
12043,15	Pigeonite	10.1	7.68	[4]	[29]	-2.45	4.78	10.0	389
14321,1246	Group A	11.3	13.9	[5]	[5]	-10.32	9.96	2.4	2501
14321,1473	Group A	11.3	11.0	[6]	[6]	-11.82	10.20	2.1	596
14321,1611	Group A	14.0	10.9	[7]	[30]	-8.91	8.76	2.7	479
14321,1763	Group A	11.6	10.9	[8]	[8]	-11.73	10.19	2.1	1215
14321,1261	Group B	12.0	9.9	[5]	[5]	-7.75	8.98	3.1	451
14321,1376	Group B	12.1	10.2	[6]	[6]	-6.28	7.80	3.9	686
14321,1475	Group B	11.6	9.37	[6]	[6]	-6.52	7.80	3.7	211
14321,1482	Group B	13.2	8.7	[6]	[6]	-7.74	8.34	3.1	476
14321,1483	Group B	14.2	7.9	[6]	[6]	-6.52	8.42	3.7	476
14321,9090	Group B	12.2	8.6	[6]	[6]	-5.90	8.27	4.1	202
14321,1476	Group C	12.1	8.48	[6]	[6]	-8.58	9.45	2.8	947
<i>14321,1608</i>	<i>Group C</i>	<i>13.6</i>	<i>8.5</i>	<i>[7]</i>	<i>[30]</i>	<i>-4.71</i>	<i>7.64</i>	<i>5.2</i>	<i>173</i>
14321,1609	Group C	12.84	9.6	[7]	[30]	-5.75	7.78	4.2	629
14321,1610	Group C	13.0	11.8	[7]	[30]	-5.48	8.11	4.4	1055
14321,9057	Group C	12.0	9.1	[8]	[8]	-6.28	8.42	3.9	210
14321,9080	Group C	12.1	10.8	[8]	[8]	-5.03	7.75	4.8	296
14053,18	Group C	12.85	8.29	[9]	[31]	-4.41	6.82	5.5	464
14072,49	High-Al	11.07	8.29	[10]	[32]	-4.84	7.76	5.0	3071
14073,16	Impact Melt	20.8	8	[12]	[34]	-3.76	7.60	6.5	2810
14276,54	Impact Melt	21.34	7.1	[11]	[35,36]	-3.87	8.11	6.3	4050
14310,175	Impact Melt	20.74	8.0	[11]	[33]	-3.00	6.69	8.1	1368
60235,17*	Impact Melt	14.94	3.43	[12]	[12]	-4.00	6.56	6.1	331
60335,13	Impact Melt	24.49	9.14	[16]	[13]	-2.71	7.37	9.0	4326
<i>60635,2</i>	<i>Impact Melt</i>	<i>26.69</i>	<i>4.92</i>	<i>[15]</i>	<i>[13]</i>	<i>-0.17</i>	<i>1.92</i>	<i>140.6</i>	<i>175</i>
65795,2	Impact Melt	27.99	3.73	[15]	[13]	-0.92	5.98	26.4	2413
67095,36	Impact Melt	19.9	13.65	[13]	[13]	-3.88	6.67	6.3	2165
67559,1	Impact Melt	24.31	4.1	[14]	[13]	-3.74	7.38	6.5	461
67559,28	Impact Melt	24.31	4.1	[14]	[13]	-3.92	7.40	6.2	755
67747,1	Impact Melt	23.1	11.34	[14]	[13]	-4.09	6.61	6.0	452
67948,14	Impact Melt	20.28	9.99	[13]	[13]	-2.29	5.82	10.6	1439
68415,141	Impact Melt	28.6	4.4	[16]	[37]	-2.10	6.14	11.6	5704
68416,126	Impact Melt	27.11	4.77	[13]	[13]	-2.76	6.57	8.8	525
65703,9-13	VLT Basalt	ND	ND	[17]	-----	-11.76	11.00	2.1	693
60639,2	Hi-Ti Basalt	11.83	6.2	[15]	[18]	-5.53	7.21	4.4	840
<i>60639,52</i>	<i>Hi-Ti Basalt</i>	<i>11.51</i>	<i>7.38</i>	<i>[18]</i>	<i>[18]</i>	<i>-6.54</i>	<i>7.30</i>	<i>3.7</i>	<i>222</i>
70135,65	Type A	7.53	10.0	[19]	[39]	-3.04	3.26	8.0	255
75015,52	Type A	10.06	6.2	[19]	[38]	-0.92	1.14	26.4	393
<i>70315,27</i>	<i>Type B1</i>	<i>9.3</i>	<i>10.0</i>	<i>[19]</i>	<i>[42]</i>	<i>-2.07</i>	<i>2.40</i>	<i>11.8</i>	<i>125</i>
<i>71557,7</i>	<i>Type B1</i>	<i>9.3</i>	<i>8.5</i>	<i>[20]</i>	<i>[20]</i>	<i>-2.02</i>	<i>2.85</i>	<i>12.1</i>	<i>101</i>
75075,86	Type B1	8.2	9.49	[19]	[38,40]	-3.28	3.66	7.4	389
78575,10	Type B1	9.0	7.5	[21]	[20,41]	-2.03	2.76	12.0	391
71035,32	Type B2	8.77	7.98	[19]	[38]	-1.66	3.84	14.7	708
74255,55	Type C	8.55	10.5	[19]	[38]	-2.71	4.50	9.0	523
79001,2187	Type D	9.3	10.9	[22]	[22]	-5.99	7.13	4.1	528

ND = No Data; Hi-Ti = High Titanium; VLT = Very Low Titanium.

Highlighted samples are those where <250 crystals are used to construct the CSD. Samples in italics are not used because of the criteria discussed in the text and in Fig. 7.

References: [1] [Beaty et al. \(1979\)](#); [2] [Dungan and Brown \(1977\)](#); [3] [Neal et al. \(1994a\)](#); [4] [Baldrige et al. \(1979\)](#); [5] [Shervais et al. \(1985b\)](#); [6] [Neal et al. \(1988a\)](#); [7] [Neal et al. \(1989a\)](#); [8] [Dickinson et al. \(1985\)](#); [9] [Taylor et al. \(2004\)](#); [10] [Longhi et al. \(1972\)](#); [11] [Gancarz et al. \(1972\)](#); [12] [Gancarz et al. \(1971\)](#); [13] [Fagan \(2012\)](#); [14] [Steele and Smith \(1973\)](#); [15] [Dowty et al. \(1974\)](#); [16] [Warner et al. \(1973\)](#); [17] [Zeigler et al. \(2006\)](#); [18] [Fagan and Neal \(2012\)](#); [19] [Brown et al. \(1975\)](#); [20] [Warner et al. \(1975a\)](#); [21] [Warner et al. \(1978\)](#); [22] [Ryder \(1990\)](#); [23] [Willis et al. \(1972\)](#); [24] [Maxwell and Wiik \(1971\)](#); [25] [Rhodes et al. \(1977\)](#); [26] [Neal et al. \(1994b\)](#); [27] [Willis et al. \(1971\)](#); [28] [Kushiro and Haramura \(1971\)](#); [29] [Snyder et al. \(1997\)](#); [30] [Neal et al. \(1989b\)](#); [31] [Ehmann et al. \(1972\)](#); [32] [Taylor et al. \(1972\)](#); [33] [Philpotts et al. \(1972\)](#); [34] [Laul et al. \(1972\)](#); [35] [Rose et al. \(1972\)](#); [36] [Warren and Wasson \(1978\)](#); [37] [Ryder and Norman \(1980\)](#); [38] [Rhodes et al. \(1976\)](#); [39] [Duncan et al. \(1976\)](#); [40] [Rhodes et al. \(1974\)](#); [41] [Laul et al. \(1975\)](#); [42] [Warner et al. \(1979\)](#).

* Represents plagioclase CSD avoiding the quench zone around xenoliths/xenocrysts.

Marsh, 1988). For plagioclase, similar criteria are followed, with the exception that the corrected crystal size range is ≥ 0.3 mm. For both olivine and plagioclase, only consecutive data points with errors $\leq 15\%$ are used to determine the slope and intercept of the CSD in these ranges. Plagioclase is volumetrically more abundant than olivine in mare basalts and impact melts, which means fewer statistically relevant olivine CSDs can be constructed relative to plagioclase.

4. RESULTS

Plagioclase and olivine CSDs for the individual samples noted in *Tables 1 and 2* are presented in *Figs. 4 and 5*, respectively. Previous studies have qualitatively shown that the plagioclase CSDs of endogenous basalts and impact melts from Apollo 14 exhibit a decreasing CSD slope from Group A to Group B to Group C and to the impact melts (*Fig 4b*; *Oshrin, 2009*; *Neal et al., 2010*; *Hui et al., 2011*). For olivine, the impact melts

appear to have steeper CSDs than those from mare basalts (see *Fig. 5a* where the impact melts are represented by the A-14 Olivine Vitrophyres; *Fagan et al., 2013a*). However, it is difficult to differentiate all sample types when CSDs are presented in this way. This paper quantifies these qualitative observations to better compare the diverse CSDs shown in *Figs. 4 and 5*.

It has been recommended that “as a minimum, 75 crystals are required to robustly define crystal habit for CSD measurements if crystals are tabular in shape, with more acicular shapes requiring a minimum of 250 sections, suggesting a sample size of >250 sections to be used for shape determination in natural examples where the true 3D shape is unknown” (*Morgan and Jerram, 2006*). With plagioclase often exhibiting an acicular habit, there are 10 samples in our database that have plagioclase CSDs defined using <250 crystals (*Table 1*; *Fig. 6*). We have evaluated these CSDs in qualitative terms using the smoothness of the profile, and in quantitative terms using the errors in population density – if they are $\leq 10\%$ for at least three consecutive

Table 2
Samples where olivine crystal size distributions have been determined for this study.

Sample #	Sample type	Al ₂ O ₃ (wt.%)	MgO (wt.%)	Petrography reference	Whole rock reference	CSD slope	CSD intercept	Residence time (yrs.)	# Of crystals
12004,137	Olivine	8.51	12.53	[1]	[14]	−6.33	4.80	1.59	143
12008,65	Ilmenite	7.98	12.33	[2]	[15]	−7.84	6.84	1.28	779
12015,29	Olivine	8.57	11.88	[3]	[15,16]	−9.37	6.62	1.07	805
12016,41	Ilmenite	7.23	12.65	[2]	[17]	−8.36	6.58	1.20	215
12020,57	Olivine	7.99	14.89	[1]	[17]	−5.86	4.56	1.72	109
14321,1260	Group A	12.4	10.7	[4]	[4]	−12.30	9.14	0.82	133
14321,1473	Group A	11.3	11.0	[5]	[5]	−11.91	9.09	0.84	233
71597,12,13*	>0.4 mm	7.9	15.8	[6]	[18]	−3.30	1.60	3.04	165@
71597,12,13*	<0.4 mm	7.9	15.8	[6]	[18]	−13.41	5.12	0.75	165@
71048,3,6	Type B1	8.7	8.0	[7]	[7]	−9.10	6.43	1.10	114
74235,60	Type A	8.61	8.35	[8]	[19]	−4.61	4.81	2.18	198
74275,312	Type C	8.72	10.36	[8]	[19]	−12.81	7.49	0.79	617
75115,4	Type B1	8.9	9.3	[8]	[20]	−2.32	4.81	4.34	83
77516,30	Type B2	7.8	9.4	[9]	[9,21]	−2.12	3.74	4.75	81
79516,9	Type B2	8.4	8.0	[10]	[10]	−5.04	4.83	2.00	91
60603,10-16	High-Ti Vit.	5.5	13.0	[11]	[11]	−56.68	13.80	0.18	695
65703,9-13	VLT	–	–	[11]	–	−24.91	9.97	0.40	168
14321,1305	Impact Melt	12.84	19.2	[12]	[12]	−31.80	11.13	0.32	254
14321,1471	Impact Melt	13.9	19.7	[13]	[22]	−28.32	11.28	0.36	844
14321.1486	Impact Melt	–	–	[13]	–	−43.09	11.49	0.23	922
14321,1602	Impact Melt	14.0	18.5	[13]	[22]	−25.07	10.10	0.40	698

@ 165 represents the total number of olivine crystals used to construct the entire CSD for 71597.

Abbreviations: Vit. = Vitrophyre; VLT = Very-low-Ti; Ol. Vit. = Olivine Vitrophyre. Whole-rock composition for 14321,1305 taken to be the same as 14321,1158 due to textural and modal similarities (*Shervais et al., 1988*).

References: [1] *Walker et al. (1976)*; [2] *Dungan and Brown (1977)*; [3] *Neal et al. (1994a)*; [4] *Shervais et al. (1985a,b)*; [5] *Neal et al. (1988a,b)*; [6] *Warner et al. (1977)*; [7] *Neal et al. (1990)*; [8] *Brown et al. (1975)*; [9] *Warner et al. (1975a)* 6th; [10] *Warner et al. (1979)*; [11] *Zeigler et al. (2006)*; [12] *Shervais et al. (1988)*; [13] *Fagan et al. (2013a)*; [14] *Maxwell and Wiik (1971)*; [15] *Rhodes et al. (1977)*; [16] *Snyder et al. (1997)*; [17] *Kushiro and Haramura (1971)*; [18] *Murali et al. (1977)*; [19] *Rhodes et al. (1976)*; [20] *Warner et al. (1975b)* MBC; [21] *Laul et al. (1975)*; [22] *Neal and Taylor (1989)*.

* Unclassified Apollo 17 basalt that has experienced accumulation of olivine (*Warner et al., 1977*). CSDs from two thin sections were combined for these samples in order to have a sufficient number of olivine crystals to make the CSD statistically relevant. The full CSD for 71597 Olivine is shown in *Fig. 4b*.

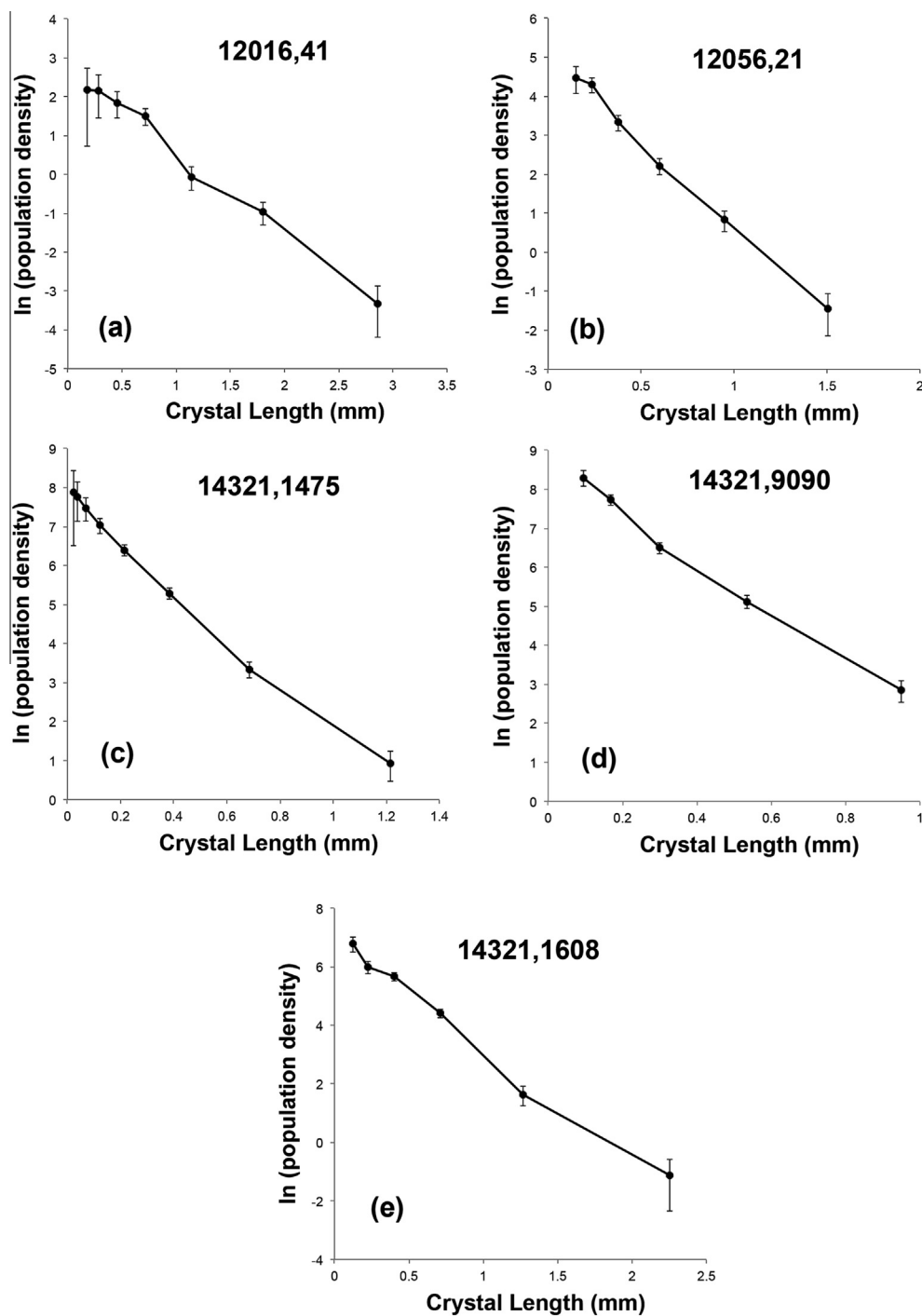


Fig. 6. Plagioclase CSDs from 10 samples where <250 crystals were used in their construction (cf. Morgan and Jerram, 2006). Each has been evaluated in a qualitative sense (e.g., smoothness of profile) and in quantitative terms (errors calculated for population density, which need to be $\leq 10\%$ for at least three consecutive data points for the profile to be used). (a) 12016,41; (b) 12056,21; (c) 14321,1475; (d) 14321,9090; (e) 14321,1608; (f) 14321,9057; (g) 60635,2; (h) 60639,52; (i) 70315,27; and (j) 71557,1. Of these 10 samples (highlighted in Table 1) only four pass both criteria and are used in this study – 12056,21; 14321,1475; 14321,9057; and 14321,9090. Six samples (12016,41; 60639,52; 14321,1608; 71557,1; 70315,27; 60635,2) were not used.

data points, the profile can be used. In order for plagioclase CSD profiles to be used in our classification scheme samples must pass both criteria. Of these 10 samples (highlighted in Table 1), 6 are not used any further in this study (12016,41; 14321,1608; 60635,2; 60639,52; 70315,27; and 71557,1). All

samples used to construct olivine CSDs (Table 2) contained >70 crystals that could be used. The smallest population used to define a plagioclase CSD is 92 (12016,41; Table 1), and for olivine it is 81 for 77516,30 (Table 2). All CSDs reported here have uncertainties that are <15%, indicating

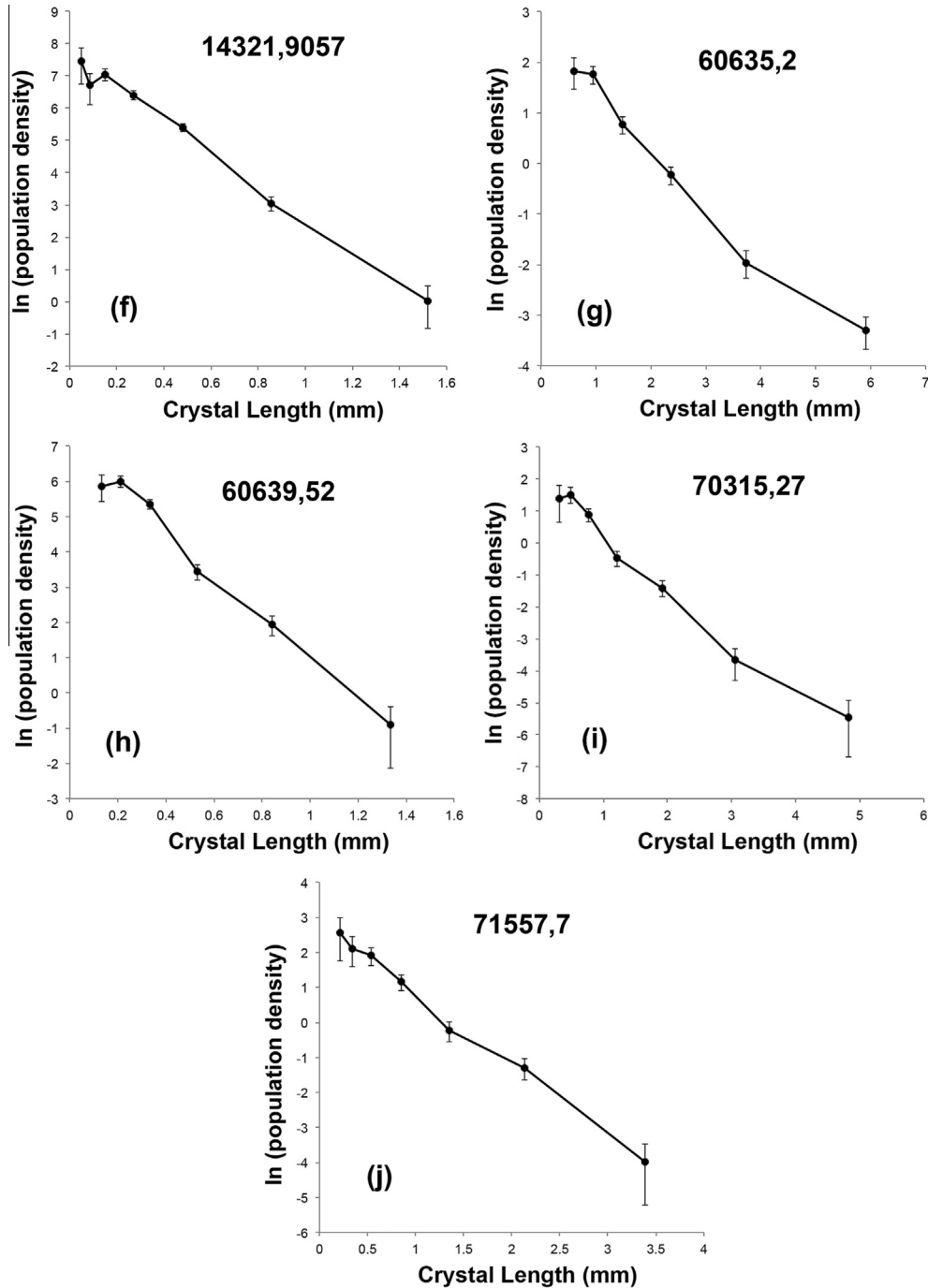


Fig 6. (continued)

a representative statistical population of crystals for each thin section was sampled.

Marsh (1998) concluded that igneous systems display a significant range of relations between CSD slope, maximum crystal size, and intercept. The CSD data presented here are depicted by plotting the slope of the CSD in the size ranges noted in the previous section against the intercept, and plotting the reciprocal of the residence time against the ratio of the slope to the intercept (Figs. 7 and 8). The residence time is related to the slope of the CSD (Fig. 3a) and a negative relationship should be evident from Figs. 7b and 8b. These

plots show how nucleation density and residence time can be used to distinguish between impact melts and pristine mare basalts.

5. DISCUSSION

5.1. Plagioclase

The plagioclase CSD data (Fig. 4) exhibit a number of features when presented on a plot of CSD Slope vs. CSD Intercept (Fig. 7a). The Apollo 14 basalts define a distinct

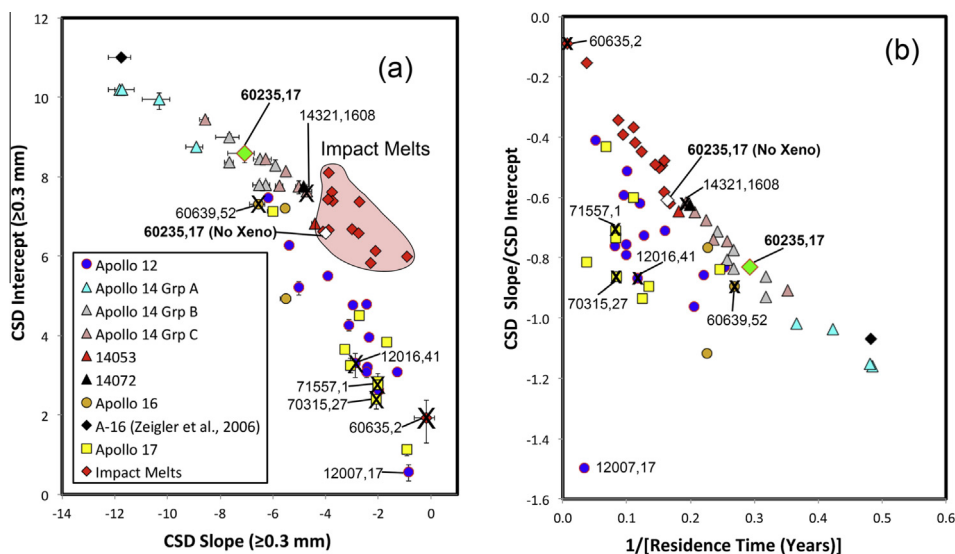


Fig. 7. Discrimination of endogenous basalts from impact melts using plagioclase CSDs. (a) Plot of CSD Slope vs. CSD Intercept for plagioclase using the criteria described in the text, with errors calculated from *CSDCorrections* shown for each data point. If error bars are not visible, they are within the size of the symbol. The impact melt field is highlighted. (b) Plot of the reciprocal of the Residence Time vs. CSD Intercept for plagioclase using the average low-pressure plagioclase growth rate of $1.304 \times 10^{-9} \text{ cm s}^{-1}$ of Burkhard (2005). In both panels the 6 samples that used <250 crystals to construct the CSD and did not meet the criteria to be used in this study (see Fig. 6 and text for discussion of these criteria) are shown with an “X” through them and are labeled.

field from the overlapping data from Apollo 12 and Apollo 17 basalts. Residence times, calculated using the average plagioclase growth rate in basaltic magmas at low pressure given in Burkhard (2005) of $1.304 \times 10^{-9} \text{ cm s}^{-1}$, show that the Apollo 14 high-Al basalts give increasing values (although overlapping) from Group A, through Groups B and C, to the impact melts (Table 1), supporting the qualitative observations of Oshrin (2009), Neal et al., 2010), and Hui et al. (2011). In general, the impact melts form a cluster of data that for a given CSD intercept have a lower CSD slope relative to mare basalts, which means that they have a higher nucleation density. They also have some of the highest residence times (Table 1; Fig. 7b). These relationships indicate that relative to the mare basalts, the impact melts have plagioclase on the liquidus for longer periods and have a higher nucleation density for this mineral relative to mare basalts.

Impact melt 60635 is an outlier of the impact melt field (Fig. 7a), having the shallowest slope and lowest intercept; this sample contains the largest plagioclase crystals of any impact melt in this study, suggesting it came from a slow cooling interior of a thick impact melt sheet. This is supported when the residence time is considered, as it yields a value of 140.5 years (Table 1). However, the CSD of 60635,2 does not meet the criteria outlined above for using the CSD in this study, and it is omitted from Fig. 7b, as are 12016,41, 14321,1608, 60639,52, 70315,27, and 71557,7, while they are marked with an “X” in Fig. 7a and b.

The Apollo 16 basalt fragment 65703,9-13 reported by Zeigler et al. (2006) has a relatively short residence time of 2.1 years and plots slightly above the Apollo 14 Group A basalts in Fig. 7a. It is unclear whether 65703,9-13 has a similar composition to the Apollo 14 Group A basalts,

or is a VLT basalt similar to those returned by Luna 24, as proposed by Zeigler et al. (2006); the only major elements reported were TiO_2 (0.5 wt.%), FeO (21.4 wt.%), CaO (12.1 wt.%), and Na_2O (0.218 wt.%). This basalt plots close to the Apollo 14 Group A high-Al mare basalts (Fig. 7a and b) and in conjunction with olivine CSD data (see below) this sample is not designated as an impact melt.

Apollo 14 Group C basalt 14053 falls close to (but not within error of – see below) the impact melt field (Fig. 7a), thus extending the trend defined by Apollo 14 high-Al basalts by plotting at the lower CSD slope end of the trend and apart from other Group C basalts. Although geochemically classified as a Group C high-Al basalt, it has been demonstrated that 14053 is unique in that the exterior surfaces are highly reduced (Mayne and Taylor, 2003; Patchen and Taylor, 2004; Taylor et al., 2004). This was caused by exposure at the lunar surface with implantation of solar wind H, followed by metamorphism via heating from being covered with an impact ejecta blanket, before re-exposure and sampling by the Apollo 14 mission. The thin section used in this study (14053,18) was one of 12 thin sections taken from potted butt 14053,2. The original chip of 14053,2 had an exterior surface on one side and fresh interior on the other. This appears to be the “recon” chip made by the Apollo 14 Preliminary Examination Team to make the initial characterization. Subsample 14053,18 was one of the last thin sections made from ,2 and it is likely that it is from the exterior portion of the sample. The CSD results are consistent with this section being taken from an area that experienced thermal metamorphism via a hot impact ejecta blanket, thus promoting some textural coarsening (i.e., growth of larger crystals at the expense of smaller ones; also known as Ostwald ripening; e.g.,

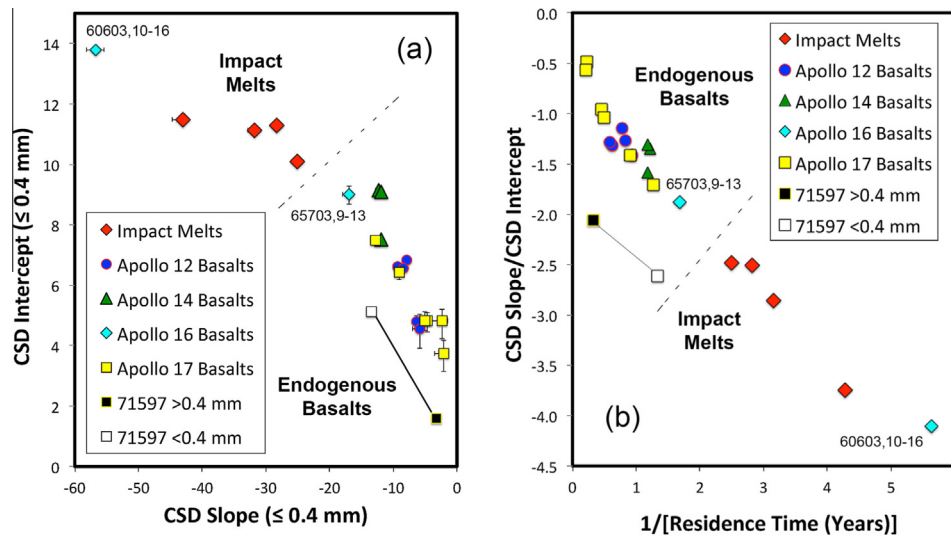


Fig. 8. Discrimination of endogenous basalts from impact melts using olivine CSDs. (a) Plot of CSD Slope vs. CSD Intercept for olivine using the criteria described in the text, with errors calculated from *CSD Corrections* shown for each data point. If error bars are not visible, they are within the size of the symbol. All data are for the CSD segments that are ≤ 0.4 mm except for one of the 71597 points, which is shown for comparison. (b) Plot of the reciprocal of the Residence Time vs. CSD Intercept for olivine using the average low-pressure olivine growth rate of $3.1623 \times 10^{-9} \text{ cm s}^{-1}$ of Borell and Kilinc (2012).

Marqusee and Ross, 1984; Voorhes, 1985, 1992) that reduces the overall CSD slope and intercept and moving 14053 closer to the impact melts in Fig. 7a.

The plagioclase CSD data are also presented in terms of the reciprocal of the residence time (Table 1) plotted against the ratio of the slope to the intercept (Fig. 7b). The impact melts plot as an extension of the Apollo 14 high-Al basalt trend, but have a higher slope to intercept ratio and a longer residence time (lower reciprocal of residence time). They are distinguished from Apollo 12 and 17 basalts, which have similar residence times but have generally lower slope/intercept ratios, although some overlap does occur (Fig. 7b). The Apollo 12 and 17 basalts exhibit less well-defined trends relative to the Apollo 14 high-Al basalts and the impact melts, and generally plot below them.

Mare basalt 12007 plots as an outlier from the rest of the Apollo 12 data in Fig. 7b. The plagioclase CSD for this sample is concave-up, but has a much lower y -axis intercept and extends to much larger crystal sizes than the other Apollo 12 basalts studied here, with the possible exception of feldspathic basalt 12038 (Fig. 4a). It is hypothesized that textural coarsening has affected this sample, reducing the slope of the CSD as well as the y -axis intercept. This can occur if the temperature is kept relatively stable near the mineral liquidus (Voorhes, 1992; Higgins, 1998, 1999, 2002b; Higgins and Roberge, 2003), which in turn implies that 12007 represents the interior of a relatively thick lava flow or sill. This is in agreement with its petrographic description as a relatively coarse grained microgabbro (e.g., Baldrige et al., 1979).

5.2. Olivine

The olivine CSDs for impact melts and endogenous mare basalts behave in the opposite sense to plagioclase

in that those from impact melts are steeper than for mare basalts (Fig. 5a). The number of samples in this part of the study is lower than for plagioclase because mare basalts and impact melts contain fewer olivines; this means fewer statistically relevant olivine CSDs can be constructed. In a plot of CSD Slope vs. CSD Intercept (Fig. 8a), the impact melts and mare basalts plot in distinct fields. Here, two Apollo 16 basalts (65703,9-13 and 60603,10-16) reported by Zeigler et al. (2006) are shown. Sample 65703,9-13 plots with the Apollo 14 Group A high-Al mare basalts (as with plagioclase in Fig. 7a), whereas 60603,10-16 extends the impact melt field to steeper negative slopes and higher y -axis intercepts (Fig. 8a).

Olivine residence times have been calculated in a similar way to those for plagioclase but using the olivine growth rate defined by Borell and Kilinc (2012) of $3.1623 \times 10^{-9} \text{ cm s}^{-1}$ (Table 2). The mare basalt olivines have the longest residence times (0.59–4.75 years) and the impact melts plus the Apollo 16 basalt 60603,10-16 have the shortest (0.2–0.4 years) (Fig. 8b). As shown in Figs. 5a and 8a, the impact melts have higher intercept (i.e., nucleation density) values and steeper CSD slopes than the mare basalts. The two Apollo 16 basalts (65703,9-13 and 60603,10-16) plot with the mare basalts and impact melts, respectively, in Fig. 8a and b, suggesting similar crystallization conditions. In Fig. 8b, the mare basalts and impact melts form a linear trend with the only exception being the olivine cumulate 71597 that falls below this trend. Conversely to the similar plot for plagioclase (Fig. 7b) the impact melts have lower olivine CSD slope/intercept ratios and shorter residence times relative to the mare basalts, although they have higher nucleation densities (Fig. 8a).

Apollo 17 high-Ti basalt 71597 is unique among the Apollo 17 mare basalt suite. It has experienced significant olivine accumulation in a high-Ti mare basalt flow

(Murali et al., 1977; Warner et al., 1977). Whole rock major and trace element analyses and major element mineral compositions indicate that 71597 experienced up to 24–27% olivine and possible minor ilmenite accumulation (Warner et al., 1977). There is a bimodal distribution of olivine Fo-content between large (~2 mm to >5 mm) subequant olivine crystals (FO_{73-79}) and smaller (0.1–0.5 mm) “matrix” olivine crystals (FO_{63-69}). The olivine CSD demonstrates this multi-modal distribution (Fig. 5b) and possibly indicates there are three groups of olivine crystals: <0.5 mm, 0.5 to 2.2 mm., and >2.2 mm; however, errors on the data points defining the larger group are beyond the 15% limit and the largest size bins could represent a continuation of the 0.5–2.2 mm trend (Fig. 5b). Therefore, 71597 is represented as two connected points on olivine CSD plots (Fig. 8a and b) solely in order to demonstrate these differences. When CSD slope and intercept are considered, both 71597 crystal populations plot within the mare basalt field (Fig. 8a).

5.3. Errors and limitations

The errors on each data point in Figs. 7a and 8a have been calculated by *CSDCorrections* (Higgins, 2000, 2002a,b; see Section 3) and error bars are presented for all data points in these diagrams. Data apparently free of error bars mean that the errors are within the size of the symbols. Inclusion of errors demonstrates that the CSD data for impact melts are distinct from those of pristine mare basalts both for olivine and plagioclase besides the stated exceptions. In addition, the CSDs for the impact melts and each mare basalt suite were constructed by six different people (coauthors on this paper), demonstrating that there is relative consistency in the way CSDs have been constructed. To illustrate this, two separate CSDs from 12038 were constructed by different people. Slopes and intercepts were calculated over approximately the same size interval (0.3–1.9 mm). Calculated slopes were -2.028 ± 0.003 and 2.180 ± 0.002 , with intercepts of 4.26 ± 0.1 and 4.16 ± 0.06 . On this basis, we submit that CSD data carefully derived from different analysts can be used to distinguish between lunar basalts derived from endogenic igneous processes and impact melt without the introduction of unacceptable errors.

Another source of error could be induced because a thin section represents a 2D slice through a 3D rock sample and one thin section may not represent the true CSD (see description in the Section 3). Therefore, plagioclase CSDs were constructed from two different thin sections of one sample, impact melt 67559 (,1 and ,28). The results indicate that the method used here yields data that are within error of each other when two sections of the same sample are examined (Fig. 9; Table 1). This allows the combination of data from two thin sections to achieve a statistically representative crystal population, which was done for 71597, a high-Ti mare basalt, by examining two thin sections (,12 and ,13; Fig. 5b).

Impact melts can be heterogeneous in nature with cooling rates highly variable at the centimeter scale if xenoliths and xenocrysts are present and have not been fully melted.

Cooling rate can have a significant effect on the slope of a CSD. In order to investigate this potential complication with the quantitative petrography method described in this paper, sample 60235 was examined in detail through analysis of thin section 60235,17 (Fig. 10). Ryder and Norman

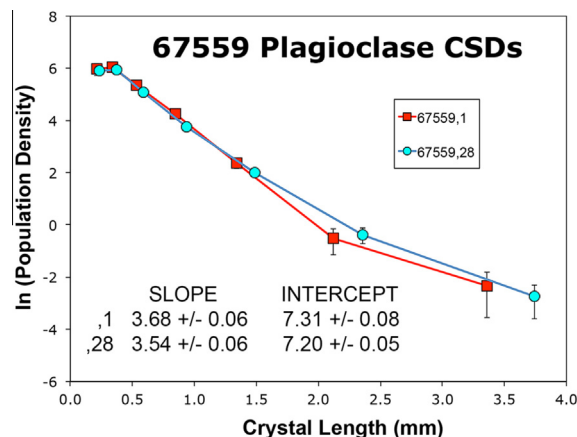


Fig. 9. Duplicate plagioclase CSDs from impact melt 67559 taken from thin sections ,1 and ,28. Both profiles are within error of each other giving confidence that the profiles taken from a single thin section of a given sample represent the crystal size distribution of the sample.

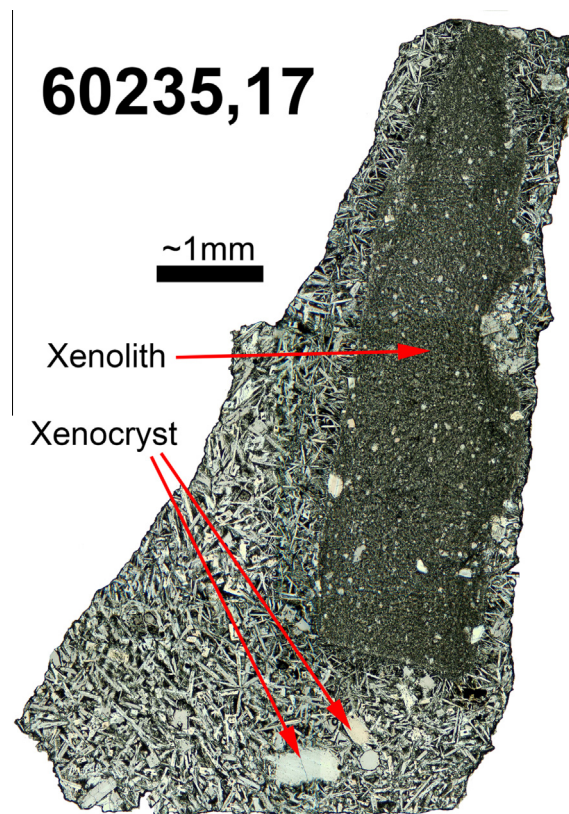


Fig. 10. Photomicrograph (in plane-polarized light) of thin section 60235,17. Note the presence of a microbreccia xenolith and two plagioclase xenoliths. There is a slight reduction in grain size of the impact melt immediately adjacent to the xenolith.

(1980) described 60235 as a plagioclase-rich impact melt containing clastic material consisting of plagioclases and plagioclase-rich breccias. This description is supported by thin section 60235,17 (Fig. 10). Crystal size distributions were constructed for all plagioclases in the melt portion of the thin section, represented by 60235,17 on Fig. 7a and b. This CSD plots within the Apollo 14 high-Al basalt field. A second plagioclase CSD was constructed omitting the plagioclases in a 0.5 mm zone around the xenolith as the grain size diminishes slightly presumably due to the cooling effect of the xenolith. This CSD is also plotted on Fig. 7a and b as 60235,17 (No Xenolith) and falls within the impact melt field. This demonstrates that impact melt cooling rates (and the slope of the plagioclase CSD profile) is influenced by the presence of xenoliths. Using the plagioclase CSD method to distinguish impact melts that contain xenoliths should be used with caution.

5.4. Influence of bulk composition

The samples analyzed in this study show distinct CSD slopes, intercepts, and residence times between impact melts and pristine mare basalts (Figs. 7 and 8). This suggests distinct crystallization regimes, which could be influenced by bulk composition. Fig. 11 is a plot of whole rock MgO (wt.%) vs. Al_2O_3 (wt.%) for all samples studied here, as they are dominated by olivine and plagioclase, respectively. The whole rock data used have the following caveats:

- Olivine vitrophyre (impact melt) 14321,1486 has no whole-rock data reported in the literature. Fagan et al. (2013a) described this as an impact melt on the basis of petrography and mineral chemistry.
- Olivine vitrophyre (impact melt) 14321,1305 (equivalent whole rock aliquot = 14321,1180) was reported by Shervais et al. (1988), but only whole-rock FeO, CaO, Na_2O , and Cr_2O_3 were reported for ,1180. However, the values for these elements are similar to those reported for olivine vitrophyre 14321,1158 (Shervais et al., 1988) whose Al_2O_3 and MgO values are adopted here to represent ,1305.
- No Al_2O_3 or MgO data were reported for 65703,9-13 (Zeigler et al., 2006).
- No MgO values have been recorded for impact melt 14073, but its Al_2O_3 content (20.8 wt.%; Laul et al., 1972) is similar to that in 14310 (20.74 wt.%; e.g., Philpotts et al., 1972), thus the same MgO value is used for 14073 (8 wt.%).

It is evident that the impact melts have distinct compositions, being either higher in Al_2O_3 or MgO (Apollo 14 olivine vitrophyres) than the pristine mare basalts (Fig. 11). Higher Al_2O_3 would enable plagioclase to be on the liquidus for a longer period of time, which is consistent with the impact melts having shallower CSD slopes and longer residence times than the mare basalts (Fig. 7). However, the shallower CSD slope may also reflect a slower

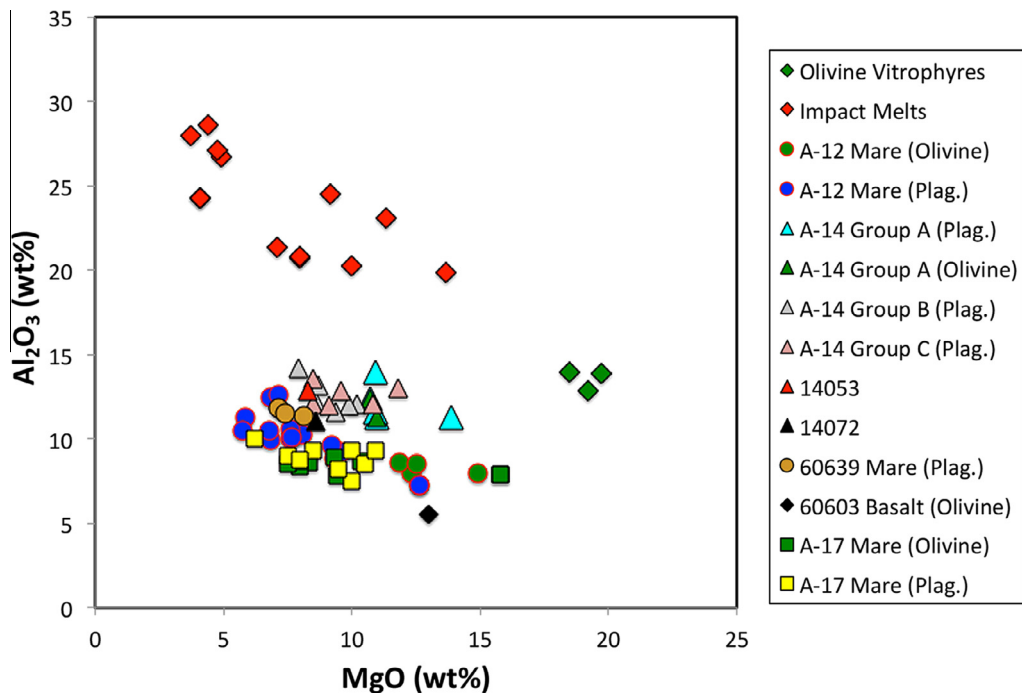


Fig. 11. Bulk rock compositions of MgO and Al_2O_3 (in wt.%) for the samples analyzed in this study. Whole rock data are from the following sources: Apollo 12 = Kushiro and Haramura (1971), Maxwell and Wiik (1971), Willis et al. (1971, 1972), Rhodes et al. (1977), Neal et al. (1994a,b), Snyder et al. (1997). Apollo 14 “14321” basalts = Dickinson et al. (1985), Shervais et al. (1985a,b), Neal et al. (1988b, 1989). 14053 = Ehmann et al. (1972). 14072 = Taylor et al. (1972). Apollo 14 impact melts = Philpotts et al. (1972), Laul et al. (1972), Rose et al. (1972), Vaniman and Papike (1980), Shervais et al. (1988), Neal and Taylor (1989). Apollo 16 basalts = Zeigler et al. (2006), Fagan and Neal (2012). Apollo 16 impact melts = Ryder and Norman (1980), Fagan et al. (2013b). Apollo 17 basalts = Rhodes et al. (1974, 1976), Laul et al. (1975), Warner et al. (1975a, 1975b, 1979), Duncan et al. (1976), Murali et al. (1977), Neal et al. (1990), Ryder (1990).

cooling rate for the impact melts relative to the mare basalts. The field of impact melts in Fig. 9 appears to form a negative correlation and suggests that bulk composition is controlling the texture. However, for olivine the impact-generated Apollo 14 olivine vitrophyres have the highest MgO, which suggests that olivine is on the liquidus for longer. This should result in shallower olivine CSD slopes and longer residence times than the mare basalts (as seen with plagioclase), but the opposite is true. In addition, Apollo 16 basaltic sample 60603,10-16 (Zeigler et al., 2006) has an olivine CSD similar to the impact melts (Fig. 8), yet its whole-rock composition is similar to the mare basalt field (Fig. 11), suggesting that whole rock composition is not controlling the olivine CSD profile.

Therefore, it is concluded that the mode of origin and cooling rate are the main factors in olivine textural development. Conversely, bulk composition may have some control over the plagioclase CSD, but our dataset suggests that mode of origin and cooling rate are also very important.

6. SUMMARY

This quantitative petrography study of lunar basaltic rocks has shown that the suite of impact melts and endogenous mare basalts analyzed as part of this study can be distinguished on the basis of plagioclase and olivine textures by using CSDs. This distinction is made using the slope and intercept of specific crystal size ranges of the CSD: ≥ 0.3 mm of plagioclase; ≤ 0.4 mm for olivine. This contradicts the findings of Higgins (2002a,b), who stated that correlation of CSD slopes and intercepts was not significant, if the volumetric phase portion is constant. The mare basalts and impact melts have overlapping modal abundance ranges: olivine in the mare basalts varies from 6 to 20 volume percent and 6 to 16 volume percent in the impact melts; plagioclase varies from 14 to 40 volume percent in the mare basalts, and 21–56 volume percent in the impact melts.

Impact melts have plagioclase and olivine CSDs that appear to give conflicting information; plagioclase impact melt CSDs generally have shallower slopes and relatively large crystal sizes relative to the mare basalts, while olivine CSDs have steeper slopes for impact melts and relatively small crystal sizes (Figs. 4 and 5). Olivine and plagioclase CSDs have been constructed for four mare basalt samples (12016,41; 14321,1473; 14321,1482; 65703,9-13) and confirm the dichotomous behavior (compare Figs. 7a and 8a). This could not be confirmed with the impact melt samples studied here as no impact melt sample permitted construction of CSDs for both plagioclase or olivine.

The dichotomous behavior between olivine and plagioclase CSDs for the mare basalts and impact melts does not appear to be controlled primarily by bulk composition. For example, mare basalt 14053 plots close to the impact melts in Fig. 7a and b, but bulk compositions appear to be distinct (Fig. 11). Apollo 16 basalt 60603,20-16 plots with the impact melts on the basis of olivine CSD data, and 65703,9-13 plots with the mare basalts on the basis of both olivine and plagioclase CSD data. This is consistent

with the findings of Donohue et al. (2013, 2014) who used mineral chemistry to define the origins of these samples.

On the basis of the quantitative petrography presented in this paper, a classification scheme that defines lunar impact melts from mare basalts is shown in Fig. 7a for plagioclase and Fig. 8a olivine CSD data. The textural classification is consistent with siderophile element abundances for the samples analyzed here (Fig. 2a and b). While further data will update the limits of these fields, the current dataset supports the initial classification of lunar basaltic samples on the basis of quantitative petrography.

6.1. Importance of this study

It is unlikely that, in the foreseeable future, hand-specimen sized extraterrestrial samples will be returned from the Moon or any other extraterrestrial planetary body. Therefore, planetary scientists must learn to work with smaller and smaller sample sizes. Destructive analyses (e.g., HSE) are not ideal methods to test if a lunar sample is of impact origin or is a product of partial melting of the lunar interior. For example, South Pole-Aitken basin sample return, with the goal of collecting SPA impact melt to age-date the basin event, is an identified mission in the latest decadal survey for NASA's Planetary Science Division (National Research Council, 2011). The current plan for this sample return mission is to return ~ 2 kg of 2–4 mm fragments high-graded from lunar regolith. Thus, it is critical to the success of such a mission that we be able to reliably distinguish between impact melts and pristine mare basalt samples. The small sample sizes would negate HSE determinations, so if a distinction can be made on the basis of petrography, more sample would be available for other studies, including geochronology. The quantitative petrography method for plagioclase and olivine described here shows promise in being able to distinguish between these two types of igneous rock and allow such a mission to achieve its science goals.

The quantitative petrography method will also open up a wealth of new research possibilities in the existing lunar sample collection. Re-examination of the 2–4 mm soil fragments returned by the Apollo and Luna missions using this method could help refine mare basalt volcanism as well as impact events. Examination of small clasts from returned breccia samples will also be possible in order to determine their impact vs. pristine origin. In essence, the quantitative petrography method can determine the origin of a clast while maximizing the amount of remaining sample for other studies.

7. CONCLUSIONS

The quantitative petrography method presented in this paper shows promise in distinguishing impact melts from endogenous melts of the lunar interior (i.e., mare basalts) using just a thin section. It first requires the construction of crystal size distributions for olivine and/or plagioclase. Analysis of known lunar impact melts and pristine mare basalts demonstrates that, at least for the samples studied here, the two origins are distinguishable using this method

(one sample, 14053 shows ambiguities in its texture that are related to post-eruption thermal metamorphism via a hot impact ejecta blanket). Specifically, olivine from impact melts displays a steeper CSD relative to olivine from mare basalts. For plagioclase, generally impacts melts display CSDs with shallower gradients than those from endogenous mare basalts and, as for olivines, plot in a distinct field on a slope vs. intercept plot. Using just a thin section to distinguish impact melts from endogenous mare basalts enables the goals of future robotic sample return missions that will potentially return small (2–4 mm) “rocklets” for analysis.

ACKNOWLEDGMENTS

This study has resulted from support to CRN through NASA Cosmochemistry Grants NNG06-GF11G and NNX09AB92G and through the NASA Lunar Science Institute contract to the Center for Lunar Science and Exploration at the Lunar and Planetary Institute, Houston with a subcontract to the University of Notre Dame (USRA sub #02173-05). Thoughtful and extremely helpful reviews from Wolf Uwe Reimold, an anonymous reviewer, and Associate Editor Christian Koeberl dramatically improved this manuscript, and the authors extend their gratitude to these people. Finally, thanks to the Apollo astronauts for collecting such an impressive sample collection, and to all the support personnel involved in making human space exploration a reality.

REFERENCES

- Allen F. M., Bence A. E. and Grove T. L. (1979) Olivine vitrophyres in Apollo 14 breccia 14321: samples of high-Mg component of the lunar highlands. In *10th Proc. Lunar Planet. Sci. Conf.* pp. 695–712.
- Anders E. (1978) Procrustean science: indigenous siderophiles in the lunar highlands, according to Delano & Ringwood. In *9th Proc. Lunar Planet. Sci. Conf.* pp. 161–184.
- Anders E., Ganapathy R., Keays R. R., Laul J. C. and Morgan J.W. (1971) Volatile and siderophile elements in lunar rocks: comparison with terrestrial and meteoritic basalts. In *2nd Proc. Lunar Sci. Conf.* pp. 1021–1036.
- Baedecker P. A., Chou C. -L. and Wasson J. T. (1972) The extralunar component in lunar soils and breccias. In *3rd Proc. Lunar Sci. Conf.* pp. 1343–1359.
- Baldrige W. S., Beaty D. W., Hill S. M. R. and Albee A. L. (1979) The petrology of the Apollo 12 pigeonite basalt suite. In *10th Proc. Lunar Planet. Sci. Conf.* pp. 141–179.
- Beaty D. W., Hill S. M. R., Albee A. L. and Baldrige W. S. (1979) Apollo 12 feldspathic basalts 12031, 12038, and 12072: petrology, comparison, and interpretation. In *10th Proc. Lunar Planet. Sci. Conf.* pp. 115–139.
- Borell A. and Kilinc A. (2012) Growth rate of olivine in a basaltic melt from the Kilauea volcano, Hawaii, using crystal size distribution theory. *Geol. Soc. Amer. Annual Mtg.* 236-3 (abstr.).
- Brown G. M., Peckett A., Emeleus C. H., Phillips R. and Pinsent R. H. (1975) Petrology and mineralogy of Apollo 17 mare basalts. In *6th Proc. Lunar Sci. Conf.* pp. 1–13.
- Burkhard D. J. M. (2005) Nucleation and growth rates of pyroxene, plagioclase, and Fe–Ti oxides in basalt under atmospheric conditions. *Eur. J. Mineral.* **17**, 675–685.
- Cashman K. V. (1990) Textural constraints on the kinetics of crystallization of igneous rocks. In *Modern Methods of Igneous Petrology, Understanding Magmatic Processes*, vol. 24 (eds. J. Nicholls and J. K. Russell), pp. 259–314. Rev. Mineral., Mineral Soc. Am., Washington, DC.
- Cashman K. V. and Marsh B. D. (1988) Crystal size distribution (CSD) in rocks and the kinetics and dynamics of crystallization II: Makaopuhi lava lake. *Contrib. Mineral. Petrol.* **99**, 292–305.
- Chanou A., Osinski G. R. and Grieve R. A. F. (2014) A methodology for the semi-automatic digital image analysis of fragmental impactites. *Meteorit. Planet. Sci.* **49**, 621–635.
- Crawford M. L. and Hollister L. S. (1974) KREEP basalt: a possible melt from the lunar interior. In *5th Proc. Lunar Sci. Conf.* pp. 399–419.
- Day J. M. D., Pearson D. G. and Taylor L. A. (2007) Highly siderophile element constraints on accretion and differentiation of the Earth–Moon system. *Science* **315**, 217–219.
- Day J. M. D., Walker R. J., James O. B. and Puchtel I. S. (2010) Osmium isotope and highly siderophile element systematics of the lunar crust. *Earth Planet. Sci. Lett.* **289**, 595–605.
- Delano J. W. and Ringwood A. E. (1978) Indigenous abundances of siderophile elements in the lunar highlands: implications for the origin of the Moon. *Moon Planets* **18**, 385–425.
- Dickinson T., Taylor G. J., Keil K., Schmitt R. A., Hughes S. S. and Smith M. R. (1985) Apollo 14 aluminous mare basalts and their possible relationship to KREEP. In *15th Proc. Lunar Planet. Sci. Conf. 15*. In *J. Geophys. Res.* **90**, pp. C365–C374.
- Donohue P. H. (2013) Origin and evolution of high-Ti mare basalts. Ph. D. dissertation, Univ. Notre Dame.
- Donohue P. H., Stevens R. E., Neal C. R. and Zeigler R. A. (2013) Testing the origins of basalt fragments from Apollo 16. *44th Lunar Planet. Sci. Conf.*, Houston, TX. #2897 (abstr.).
- Donohue P. H., Neal C. R., Stevens R. E. and Zeigler R. A. (2014) Crystal stratigraphy of two basalts from Apollo 16: unique crystallization of picritic basalt 60603, 10-16 and very-low-titanium basalt 65703,9-13. *45th Lunar Planet. Sci. Conf.* Houston, TX. #2648 (abstr.).
- Dowty E., Keil K. and Prinz M. (1974) Igneous rocks from Apollo 16 rake samples. In *5th Proc. Lunar Sci. Conf.* pp. 431–445.
- Dungan M. A. and Brown R. W. (1977) The petrology of the Apollo 12 ilmenite basalt suite. In *8th Proc. Lunar Sci. Conf.* pp. 1339–1381.
- Duncan A. R., Erlank A. J., Sher M. K., Abraham Y. C., Willis J. P. and Ahrens L. H. (1976) Some trace element constraints on lunar basalt petrogenesis. In *7th Proc. Lunar Sci. Conf.* pp. 1659–1671.
- Ebihara M., Wolf R., Warren P. H. and Anders E. (1992) Trace elements in 59 mostly highland Moon rocks. In *22nd Proc. Lunar Planet. Sci. Conf.* pp. 417–426.
- Ehmann W. D., Gillum D. E. and Morgan J. W. (1972) Oxygen and bulk element composition studies of Apollo 14 and other lunar rocks and soil. In *3rd Proc. Lunar Sci. Conf.* pp. 1149–1160.
- Fagan A. L. (2012) Volcanic and impact processes on Mars and the Moon. Ph. D. dissertation, Univ. Notre Dame. pp. 259.
- Fagan A. L. and Neal C. R. (2012) Apollo 11-type basalts from Apollo 16: a new type of high-Ti basalt? *43rd Lunar Planet. Sci. Conf.*, Houston, TX. #1429 (abstr.).
- Fagan A. L., Neal C. R., Simonetti A., Donohue P. H. and O’Sullivan K. M. (2013a) Distinguishing between Apollo 14 impact melt and pristine mare basalt samples by geochemical and textural analyses of olivine. *Geochim. Cosmochim. Acta* **106**, 429–445.
- Fagan A. L., Neal C. R., Beard S. P. and Swindle T. D. (2013b) Bulk composition and ^{40}Ar – ^{39}Ar age dating suggests impact melt sample 67095 may be exotic to the Apollo 16 site. *44th Lunar Planet. Sci. Conf.*, Houston, TX. #3075 (abstr.).
- Fischer-Godde M. and Becker H. (2012) Osmium isotope and highly siderophile element constraints on ages and nature of

- meteoritic components in ancient lunar impact rocks. *Geochim. Cosmochim. Acta* **77**, 135–156.
- Gancarz A. J., Albee A. L. and Chodos A. A. (1971) Petrologic and mineralogic investigation of some crystalline rocks returned by the Apollo 14 mission. *Earth Planet. Sci. Lett.* **12**, 1–18.
- Gancarz A. J., Albee A. L. and Chodos A. A. (1972) Comparative petrology of Apollo 16 sample 68415 and Apollo 14 samples 14276 and 14310. *Earth Planet. Sci. Lett.* **16**, 307–330.
- Hertogen J., Janssens M. -R., Takahashi H., Palme H. and Anders E. (1977) In *8th Proc. Lunar Sci. Conf.* pp. 17–45.
- Higgins M. D. (1996) Magma dynamics beneath Kameni volcano, Thera, Greece, as revealed by crystal size and crystal shape measurements. *J. Volcanol. Geotherm. Res.* **70**, 37–48.
- Higgins M. D. (1998) Origin of anorthosite by textural coarsening: quantitative measurements of a natural sequence of textural development. *J. Petrol.* **39**, 1307–1323.
- Higgins M. D. (1999) Origin of megacrysts in granitoids by textural coarsening: a crystal size distribution (CSD) study of microcline in the Cathedral Peak Granodiorite, Sierra Nevada, California. In *Understanding granites: integrating modern and classical techniques*, vol. 158 (eds. C. Fernandez and A. Castro), pp. 207–219. *Understanding granites: integrating modern and classical techniques*. Geol. Soc. Lond. Spec. Publ..
- Higgins M. D. (2000) Measurement of crystal size distributions. *Am. Mineral.* **85**, 1105–1116.
- Higgins M. D. (2002a) Closure in crystal size distributions (CSD), verification of CSD calculations, and the significance of CSD fans. *Am. Mineral.* **87**, 171–175.
- Higgins M. D. (2002b) A crystal size-distribution study of the Kigplait layered mafic intrusion, Labrador, Canada: evidence for textural coarsening. *Contrib. Mineral. Petrol.* **144**, 314–330.
- Higgins M. D. and Chandrasekharam D. (2007) Nature of sub-volcanic magma chambers, Deccan Province, India: evidence from quantitative textural analysis of plagioclase megacrysts in the Giant Plagioclase Basalts. *J. Petrol.* **48**, 885–900.
- Higgins M. D. and Roberge J. (2003) Crystal size distributions of plagioclase and amphibole from Soufrière Hills volcano, Montserrat: evidence for dynamic crystallization – textural coarsening cycles. *J. Petrol.* **44**, 1401–1411.
- Hubbard N. J., Gast P. W., Rhodes J. W., Bansal B. M., Wiesmann H. and Church S. E. (1972) Nonmare basalts: Part II. In *3rd Proc. Lunar Sci. Conf.* pp. 1161–1179.
- Hui H., Oshrin J. and Neal C. R. (2011) Investigation into the petrogenesis of Apollo 14 high-alumina basaltic melts through textural and compositional analyses. *Geochim. Cosmochim. Acta* **75**, 6439–6460.
- Krahenbuhl U., Ganapathy R., Morgan J. W. and Anders E. (1973) Volatile elements in Apollo 16 samples: implications for highland volcanism and accretion history of the Moon. In *4th Proc. Lunar Sci. Conf.* pp. 1325–1348.
- Kushiro I. and Haramura H. (1971) Major element variation and possible source material of Apollo 12 crystalline rocks. *Science* **171**, 1235–1237.
- Laul J. C., Wakita H., Showalter D. L., Boynton W. V. and Schmitt R. A. (1972) Bulk, rare earth, and other trace elements in Apollo 14 and 15 and Luna 16 samples. In *3rd Proc. Lunar Sci. Conf.* pp. 1181–1200.
- Laul J. C., Schmitt R. A., Robyn M. and Goles G. G. (1975) Chemical composition of 18 Apollo 17 rake basalts and one basalt-breccia. *Lunar Planet. Sci.* **VI**, 492–494.
- Lofgren G. E. (1977) Dynamics crystallization experiments bearing on the origin of textures in impact-generated liquids. In *8th Proc. Lunar Sci. Conf.* pp. 2079–2095.
- Longhi J., Walker D. and Hays J. F. (1972) Petrography and crystallization history of basalts 14310 and 14072. In *3rd Proc. Lunar Sci. Conf.* pp. 131–139.
- Marqusee J. A. and Ross J. (1984) Theory of Ostwald ripening: competitive growth and its dependence on volume fraction. *J. Chem. Phys.* **80**, 536–543.
- Marsh B. D. (1988) Crystal size distribution (CSD) in rocks and kinetics and dynamics of crystallization I. Theory. *Contrib. Mineral. Petrol.* **99**, 277–291.
- Marsh B. D. (1996) Solidification fronts and magmatic evolution. *Mineral. Mag.* **60**, 5–40.
- Marsh B. D. (1998) On the interpretation of crystal size distributions in magmatic systems. *J. Petrol.* **39**, 553–599.
- Marsh B. D. (2002) On bimodal differentiation by solidification front instability in basaltic magmas, part I: Basic mechanics. *Geochim. Cosmochim. Acta* **66**, 2211–2229.
- Maxwell J. A. and Wiik H. B. (1971) Chemical compositions of Apollo 12 lunar samples 12004, 12033, 12051, 12052, and 12065. *Earth Planet. Sci. Lett.* **10**, 285–288.
- Mayne R. G. and Taylor L. A. (2003) New insights into the origin of 14053 – the only basaltic rock returned Apollo 14. *Lunar Planet. Sci. XXXIV*. #1604 (abstr.).
- Morgan D. J. and Jerram D. A. (2006) On estimating crystal shape for crystal size distribution analysis. *J. Volcanol. Geotherm. Res.* **154**, 1–7.
- Morgan J. W., Ganapathy R., Higuchi H., Krähenbuhl U., and Anders E. (1974) Lunar basins: Tentative characterization of projectiles from meteoritic elements in Apollo 17 boulders. In *5th Proc. Lunar Sci. Conf.* pp. 1703–1736.
- Morgan J. W., Laul J. C., Krahenbuhl U., Ganapathy R., and Anders E. (1972) Major impacts on the Moon: Characterization from trace elements in Apollo 12 and 14 samples. In *3rd Proc. Lunar Sci. Conf.* pp. 1377–1395.
- Murali A. V., Ma M.-S., Schmitt R. A., Warner R. D., Keil K. and Taylor G. J. (1977) Chemistry of 30 Apollo 17 rake samples; 71597 a product of partial olivine accumulation. *Lunar Planet. Sci. VIII*, 703–705.
- National Research Council (2007) The Scientific Context for Exploration of the Moon. 120 pp, ISBN: 0-309-10920-5. Available from: <http://www.nap.edu/catalog/11954.html>.
- National Research Council (2011) Vision and Voyages for Planetary Science in the Decade 2013-2022. Committee on the Planetary Science Decadal Survey, National Academies, 423 pp.
- Neal C. R. (2001) Interior of the Moon: the presence of garnet in the primitive deep lunar mantle. *J. Geophys. Res.* **106**, 27865–27885.
- Neal C. R. and Kramer G. Y. (2006) The petrogenesis of Apollo 14 high-Al mare basalts. *Amer. Mineral.* **91**, 1521–1535.
- Neal C. R. and Taylor L. A. (1989) Metasomatic products of the Lunar Magma Ocean: the role of KREEP dissemination. *Geochim. Cosmochim. Acta* **53**, 529–541.
- Neal C. R., Taylor L. A. and Lindstrom M.M. (1988a) The importance of Lunar Granite and KREEP in Very High Potassium (VHK) basalt petrogenesis. In *18th Proc. Lunar Planet. Sci. Conf.* pp. 121–137.
- Neal C. R., Taylor L. A., and Lindstrom M. M. (1988b) Apollo 14 mare basalt petrogenesis: Assimilation of KREEP-like components by a fractionating magma. In *18th Proc. Lunar Planet. Sci. Conf.* pp. 139–153.
- Neal C. R., Taylor L. A. and Patchen, A. D. (1989a) High alumina (HA) and very high potassium (VHK) basalt clasts from Apollo 14 breccias, part 1 – mineralogy and petrology; Evidence of crystallization from evolving magmas. In *19th Proc. Lunar Planet. Sci. Conf.* pp. 137–146.
- Neal C. R., Taylor L. A., Patchen A. D., Schmitt R. A., Hughes, S. S. and Lindstrom, M. M. (1989b) High alumina (HA) and very high potassium (VHK) basalt clasts from Apollo 14 breccias, part 2 – whole-rock geochemistry; Further evidence for

- combined assimilation and fractional crystallization within the Lunar crust. In *19th Proc. Lunar Planet. Sci. Conf.* pp. 147–162.
- Neal C. R., Taylor L. A., Hughes S. S. and Schmitt R. A. (1990) The significance of fractional crystallization in the petrogenesis of Apollo 17 Type A and Type B high-Ti basalts. *Geochim. Cosmochim. Acta* **54**, 1817–1833.
- Neal C. R., Hacker M. D., Snyder G. A., Taylor L. A., Liu Y.-G. and Schmitt R. A. (1994a) Basalt generation at the Apollo 12 site, Part I: new data, classification, and re-evaluation. *Meteoritics* **29**, 334–348.
- Neal C. R., Hacker M. D., Taylor L. A., Schmitt R. A. and Liu Y.-G. (1994b) Basalt generation at the Apollo 12 site, part 2: source heterogeneity, multiple melts, and crustal contamination. *Meteoritics* **29**, 349–361.
- Neal C.R., Fagan A.L., and Oshrin J.C. (2010) Differentiating between pristine mare basalts and impact melts using quantitative petrography. *41st Lunar Planet. Sci. Conf.*, Houston TX, # 1647 (abstr.).
- O’Sullivan K. M. (2012) Petrogenesis of planetary basalts using crystal stratigraphy. PhD dissertation, University of Notre Dame. p. 201.
- Oshrin J. (2009) *Investigation into the Petrogenesis of Apollo 14 High-Alumina Basalts through Textural and Compositional Analyses*. Masters Thesis, Univ. Notre Dame, 130 pp.
- Oshrin J. and Neal C.R. (2009) Crystal size distributions and basalt evolution: More from Fra Mauro. *40th Lunar Planet. Sci. Conf.*, Houston TX, # 1706 (abstr.).
- Palme H., Baddenhausen H., Blum K., Cendales M., Dreibus G., Hofmeister H., Kruse H, Palme C., Spettel B., Vilseck E. and Wanke H. (1978) New data on lunar samples and achondrites and a comparison of the least fractionated samples from the Earth, the Moon, and the eucrite parent body. In *9th Proc. Lunar Planet. Sci. Conf.* pp. 25–57.
- Patchen A.P. and Taylor L.A. (2004) The most reduced rock from the Moon – Apollo 14 basalt 14053: Extreme reduction entirely from a reheating event. *Lunar Planet. Sci. XXXV*, #1762 (abstr.).
- Peterson T. D. (1996) A refined technique for measuring crystal size distributions in thin section. *Contrib. Mineral. Petrol.* **124**, 395–405.
- Philpotts J. A., Schnetzler C. C., Nava D. F., Bottino M. L., Fullagar P. D., Thomas H. H., Schuhmann S. and Kouns C. W. (1972) Apollo 14: Some geochemical aspects. In *3rd Proc. Lunar Sci. Conf.* pp. 1293–1305.
- Pittarello L. and Koeberl C. (2013) Clast size distribution and quantitative petrography of shocked and unshocked rocks from the El’gyygtyn impact structure. *Meteorit. Planet. Sci.* **48**, 1325–1338.
- Puchtel I. S., Walker R. J., James O. B. and Kring D. A. (2008) Osmium isotope and highly siderophile element systematics of lunar impact melt breccias: implications for the late accretion history of the Moon and Earth. *Geochim. Cosmochim. Acta* **72**, 3022–3042.
- Rasband, W.S., (1997) ImageJ. *U. S. National Institutes of Health*, Bethesda, Maryland, USA. Available from: <http://imagej.nih.gov/ij/> (August 21, 2013).
- Rhodes J. M., Rodgers K. V., Shih C., Bansal B. M., Nyquist L. E., Wiesmann H. and Hubbard N. J. (1974) The relationships between geology and soil chemistry at the Apollo 17 landing site. In *5th Proc. Lunar Sci. Conf.* pp. 1097–1117.
- Rhodes J. M., Hubbard N. J., Wiesmann H., Rodgers K. V., Brannon J. C. and Bansal B. M. (1976) Chemistry, classification, and petrogenesis of Apollo 17 mare basalts. In *7th Proc. Lunar Sci. Conf.* pp. 1467–1489.
- Rhodes J. M., Blanchard D. P., Dungan M. A., Brannon J. C. and Rodgers K. V. (1977) Chemistry of Apollo 12 mare basalts: Magma types and fractionation processes. In *8th Proc. Lunar Sci. Conf.* pp. 1305–1338.
- Ridley W. I., Brett R., Williams R. J., Takeda H. and Brown R. W. (1972) Petrology of Fra Mauro basalt 14310. In *3rd Proc. Lunar Sci. Conf.* pp. 159–170.
- Righter K., Walker R. J. and Warren P. H. (2000) Significance of highly siderophile elements and osmium isotopes in the lunar and terrestrial mantles. In *Origin of the Earth and Moon*, (eds. K. Righter and R. Canup). pp. 291–322.
- Rose H. J., Cuttitta F., Anell C. S., Carron M. K., Christian R. P., Dwornik E. J., Greenland L. P. and Ligon D. T. Jr. (1972) Compositional data for twenty-one Fra Mauro lunar materials. In *3rd Proc. Lunar Sci. Conf.* pp. 1215–1229.
- Ryder G. (1990) A distinct variant of high-titanium mare basalt from the Van Serg core, Apollo 17 landing site. *Meteoritics* **25**, 249–258.
- Ryder G. and Norman M. D. (1980) Catalog of Apollo 16 rocks, Part 3: 67015–69965. *NASA JSC Curatorial Branch*, Publication 52, JSC 16904, 371 pp.
- Shervais J. W., Taylor L. A., Lail J. C., Shih C. -Y. and Nyquist L. E. (1985a) Very High Potassium (VHK) basalt: Complications in mare basalt petrogenesis. In *16th Proc. Lunar Planet. Sci. Conf.*, in *J. Geophys. Res.* **90**, D3-D18.
- Shervais J. W., Taylor L. A. and Lindstrom M. M. (1985b) Apollo 14 mare basalts: Petrology and geochemistry of clasts from consortium breccia 14321. In *15th Proc. Lunar Planet. Sci. Conf.*, in *J. Geophys. Res.* **90**, C375–C395.
- Shervais J. W., Taylor L. A. and Lindstrom M. M. (1988) Olivine vitrophyres: A nonpristine high-Mg component in lunar breccia 14321. In *18th Proc. Lunar Planet. Sci. Conf.* pp. 45–57.
- Shimamoto T. and Nagahama H. (1992) An argument against the crush origin of pseudotachylytes based on the analysis of clast-size distribution. *J. Struct. Geol.* **14**, 999–1006.
- Snyder G. A., Neal C. R., Taylor L. A. and Halliday A. N. (1997) Anatexis of lunar cumulate mantle in time and space. Clues from trace-element, strontium, and neodymium isotopic chemistry of parental Apollo 12 basalts. *Geochim. Cosmochim. Acta* **61**, 2731–2747.
- Steele I. M. and Smith J. V. (1973) Mineralogy and petrology of some Apollo 16 rocks and fines: General petrologic model of Moon. In *4th Proc. Lunar Sci. Conf.* pp. 519–536.
- Taylor L. A., Patchen A., Mayne R. G. and Taylor D.-H. (2004) The most reduced rock from the Moon, Apollo 14 basalt 14053: its unique features and their origin. *Amer. Mineral.* **89**, 1617–1624.
- Taylor S. R., Kaye M., Muir P., Nance W., Rudowski R. and Ware N. (1972) Composition of the lunar uplands: Chemistry of Apollo 14 samples from Fra Mauro. In *3rd Proc. Lunar Sci. Conf.* pp. 1231–1249.
- Tsutsumi A. (1999) Size distribution of clasts in experimentally produced pseudotachylytes. *J. Struct. Geol.* **21**, 305–312.
- Usselman. T. M. and Lofgren G. E. (1976) The phase relations, textures, and mineral chemistries of high-titanium mare basalts as a function of oxygen fugacity and cooling rate. In *7th Proc. Lunar Sci. Conf.* pp. 1345–1363.
- Vaniman D. T. and Papike J. J. (1980) Lunar highland melt rocks: Chemistry, petrology and silicate mineralogy. In *Proc. Conf. Lunar Highlands Crust* (eds. J. J. Papike and R. B. Merrill). pp. 271–337. Pergamon.
- Voorhes P. W. (1985) The theory of Ostwald Ripening. *J. Statist. Phys.* **38**, 231–252.
- Voorhes P. W. (1992) Ostwald Ripening of two-phase mixtures. *Ann. Rev. Mater. Sci.* **22**, 197–215.
- Walker D., Longhi J., Kirkpatrick R.J., and Hays J.F. (1976) Differentiation of an Apollo 12 picrite magma. *7th Proc. Lunar Sci. Conf.* pp. 1365–1389.

- Walker R. J., Horan M. F., Shearer C. K. and Papike J. J. (2004) Low abundances of highly siderophile elements in the lunar mantle: evidence for prolonged late accretion. *Earth Planet. Sci. Lett.* **224**, 399–413.
- Warner R. D., Simonds C. H. and Phinney W. C. (1973) Apollo 16 rocks: Classification and petrogenetic model. In *4th Proc. Lunar Sci. Conf.* pp. 481–504.
- Warner R. D., Keil K., Muralli A. V. and Schmitt R. A. (1975a) Petrogenetic relationships among Apollo-17 mare basalts. In *Papers Presented to the Conference of the Origins of Mare Basalts and Their Implications for Lunar Evolution*, pp. 179–183. The Lunar Science Institute, Houston.
- Warner R. D., Keil K., Prinz M., Lau J. C., Murali A. V. and Schmitt R. A. (1975b) Mineralogy, petrology, and chemistry of mare basalts from Apollo 17 rake samples. In *9th Proc. Lunar Sci. Conf.* pp. 193–220.
- Warner R. D., Keil K. and Taylor G. J. (1977) Coarse-grained basalt 71597: A product of partial olivine accumulation. In *8th Proc. Lunar Sci. Conf.* pp. 1429–1442.
- Warner R. D., Taylor G. J., Conrad G. H., Northrop H. R., Barker S., Keil K., Ma M. -S. and Schmitt R. A. (1979) Apollo 17 high-Ti mare basalts: New bulk compositional data, magma types, and petrogenesis. In *10th Proc. Lunar Planet. Sci. Conf.* pp. 225–247.
- Warren P. H. (1993) A concise compilation of petrologic information on possibly pristine nonmare Moon rocks. *Amer. Mineral.* **78**, 360–376.
- Warren P. H. and Wasson J. T. (1978) Compositional-petrographic investigation of pristine non-mare rocks. In *9th Proc. Lunar Planet. Sci. Conf.* pp. 185–217.
- Warren P. H. and Wasson J. T. (1977) Pristine nonmare rocks and the nature of the lunar crust. In *8th Proc. Lunar Sci. Conf.* pp. 2215–2235.
- Willis J. P., Ahrens L. H., Danchin R. V., Erlank A. J., Gurney J. J., Hofmeyr P. K., McCarthy T. S. and Orren M. J. (1971) Some inter-element relationships between lunar rocks and fines, and stony meteorites. In *2nd Proc. Lunar Sci. Conf.* pp. 1123–1138.
- Willis J. P., Erlank A. J., Gurney J. J., Theil R. H. and Ahrens L. H. (1972) Major, minor, and trace element data for some Apollo 11, 12, 14, and 15 samples. In *3rd Proc. Lunar Sci. Conf.* pp. 1269–1273.
- Wolf R., Woodrow A. and Anders E. (1979) Lunar basalts and pristine highland rocks: Comparison of siderophile and volatile elements. In *10th Proc. Lunar Planet. Sci. Conf.* pp. 2107–2130.
- Zeigler R. A., Korotev R. L., Haskin L. A., Jolliff B. L. and Gillis J. J. (2006) Petrography and geochemistry of five new Apollo 16 mare basalts and evidence for post-basin deposition of basaltic material at the site. *Meteorit. Planet. Sci.* **41**, 263–284.

Associate editor: Christian Koeberl